ADDIS ABABA UNIVERSITY

ADDIS ABABA INSTITUTE OF TECHNOLOGY

SCHOOL OF MECHANICAL AND INDUSTRIAL ENGINEERING

MECHANICL DESIGN STREAM

Numerical investigation of fatigue growth rate and fracture lifetime Estimation of Kaplan hydraulic turbine runner blade

By: Damena Negash

A thesis submitted to the School of Graduate Studies of Addis Ababa University in partial fulfillment of the requirements of the Degree of Masters of Science in Mechanical Engineering (Mechanical Design Stream)

Advisor

Dr. Hailemariam N. Hailu

December, 2024 G.C

Addis Ababa, Ethiopia

ADDIS ABABA UNIVERSITY

ADDIS ABABA INSTITUTE OF TECHNOLOGY

SCHOOL OF MECHANICAL AND INDUSTRIAL ENGINEERING

MECHANICL DESIGN STREAM

Numerical investigation of fatigue growth rate and fracture lifetime Estimation of Kaplan hydraulic turbine runner blade

By: Damena Negash

Approved By Board of Examiners:

Dr. Hailemariam N. Hailu	_____	_____
Advisor	Signature	Date
Dr. Mulugeta Habtemariam	_____	_____
Internal Examiner	Signature	Date
Dr. Araya Abera	_____	_____
External Examiner	Signature	Date
Dr. Sosina Mengistu	_____	_____
Associate Director for Postgraduate program	Signature	Date

SIGNED DECLARATION

I declare that the thesis submitted for my M.Sc. degree at the University of Addis Ababa is my original work and has not been submitted for any degree at this or any other institution. All reference materials used are properly acknowledged.

Name: Damena Negash

Place: Addis Ababa, Ethiopia

Date of Submission: _____

Signature: _____

This is to certify that the above declaration made by the candidate is correct to the best of my Knowledge.

Dr. Hailemariam N. Hailu	_____	_____
Advisor	Signature	Date

Acknowledgment

First and foremost, I want to express my deepest gratitude to God for blessing me with amazing and generous people throughout this journey. I also want to extend my heartfelt appreciation to my advisor, Dr. Hailemariam N. Hailu. His ongoing encouragement and patient guidance have been invaluable to me. Dr. Hailu's extensive knowledge of Fracture Mechanics and its applications, combined with his infectious enthusiasm, has greatly enriched my experience as a graduate student. His patience in helping me understand the basics and his endless supply of intriguing ideas have made a significant impact on my work. I am especially thankful for his ability to inspire me and spark my interest in focusing my thesis on fracture mechanics.

I also want to extend my sincere thanks to Dr. Mulugeta Habtemariam for his valuable input during the research and writing of this thesis. His helpful comments and insightful feedback were greatly appreciated and significantly contributed to the quality of my work.

Finally, I want to express my deepest gratitude to my family and friends for their unwavering support and understanding. Their encouragement, love, and belief in me have been crucial throughout this journey. They have provided a solid foundation of emotional and practical support, which has been essential for the completion of this work. Without their constant backing and motivation, this thesis would not have been possible. Their understanding during the challenging times and their celebrations during the successes have meant more to me than words can convey. Thank you for being there every step of the way.

Table of Contents

List of Figures

List of Table

List of abbrevations

NACA	National Advisory Committee for Aeronautics
CFD	Computational Fluid Dynamics
LEFM	Linear Elastic Fracture Mechanics
EPFM	Elastic Plastic Fracture Mechanics
SNL	Speed-No-Load
PL	Part Load
SEM	Scanner Electron Microscopy
SIF	Stress Intensity Factor
SIFc	Critical Stress Intensity Factor
CTOD	Crack-Tip Opening Displacement
ASTM	American Society for Testing and Materials
FEA	Finite Element Analysis
STEP	Standard for the Exchange of Product model data

Abstract

Kaplan turbines are the most widely used hydraulic turbines around the world. Suitable for low head and high flow conditions. With these specific features Water sources are known for their efficiency in producing electricity. Kaplan turbine failures are often related to material defects, design flaw, Manufacturing errors, corrosion, fatigue, cavity wear, water erosion. The purpose of this thesis is to estimate the fracture life of Kaplan turbine blades by analyzing the growth rate of fatigue cracks. This includes the derivation of the governing equations for crack initiation, propagation and age estimation as well as designing Kaplan turbine blades. The model is developed and analyzed using ANSYS 2020R1 followed by static stress analysis and fatigue crack growth rate investigation using stress intensity factor and J-integral. The stress-intensity factor is evaluated for each increase in crack depth and is related to the growth rate of fatigue cracks. The lifespan of the fatigue rate and fracture life of runner blades is then calculated based on this relationship. Based on the result obtained, analysis of the fatigue crack growth rate and the estimated fracture life of runner blades are discussed and some recommendation have been discussed for further study.

Key word: kaplan turbine, Fatigue, fracture, runner blade, stress- intensity factor

Chapter One

1. Introduction

1.1 Background

Hydroelectric power harnesses energy from moving water, making it an important source of renewable resources. It comes from the water cycle created from solar energy where water circulates between the earth and the atmosphere. Hydropower provides a reliable source of energy despite the scarcity of other resources [1].

Hydroelectric power, generated from the energy of moving water, provides a source of renewable energy using rivers and streams that are recharged by rain and snowmelt [2].

Hydropower harnessed from water through hydroelectric dams is a clean and environmentally friendly energy solution. Providing affordable electricity while reducing carbon emissions Hydropower is a highly efficient and widely accessible renewable resource for generating electricity using energy from flowing water. Its high energy density makes it a key player in the transition to sustainable energy. It creates a green and environmentally friendly electrical grid [3]. Kaplan water turbines are important in hydroelectric power plants. It is designed to efficiently convert energy from flowing water into mechanical energy. Turbine blades critical to this conversion process are subjected to significant operating stresses and cyclic loads. As time passes these conditions can induce fatigue and cause cracks. This can affect the structural integrity and performance of the turbine.

Studying fatigue growth and fracture mechanisms is also important to enhance the lifespan and safety predictions of these turbine components. Traditional methods for evaluating blade durability usually involve empirical testing and physical inspection. This can be time-consuming and expensive. However, recent advances in computational methods offer more efficient ways to model and simulate the complex stress distribution and fatigue behavior experienced by blades.

This thesis presents a comprehensive numerical investigation aimed at understanding the fatigue growth rate and estimate the fracture life of Kaplan turbine blades.

Over View of Kaplan Turbine runner blade Technology

Kaplan turbines, which are required in hydroelectric systems. Use adjustable rotor speed to optimize performance under various driving conditions. These plates are designed to efficiently convert water flow into mechanical energy. The project covered complex hydrodynamic principles and computational methods such as Computational Fluid Dynamics (CFD) to optimize efficiency and performance [4]. Material selection is critical for durability. They are usually made of high-strength steel and composite materials to resist wear, corrosion, and cavitation [5]. But Kaplan turbine blades are also subject to fatigue due to cyclic loading. This requires regular maintenance and inspection to guarantee reliability and extend its life [6].

Recent advances include the integration of real-time monitoring systems and advanced numerical modeling techniques to predict better performance and longevity of the repair [7]. These innovations have helped increase turbine efficiency and reduced maintenance costs highlighting the importance of continuous technological development in Kaplan's turbine technology. This research carried out a numerical study of the fatigue growth rate and fracture life estimation of Kaplan's hydraulic turbine blades.

Causes of damages Kaplan turbine blade

Kaplan turbines are popular hydraulic turbines used in areas with low water levels and high flow rates. If some turbines parts breaks, it will cause significant downtime and expensive repairs. In some cases, if a broken plate damages other parts, such as the main floor, the entire plant may be temporarily closed [8]. Turbine failure is a result of material flow, design flaw, manufacturing defects, corrosion, fading, cavitation wear and different types of cavitation in hydroelectric turbines. Problems such as water corrosion also contribute to their failure. Material defects and design flaws can affect the integrity of the turbine. while manufacturing defects affect performance. Cavitation wear is caused by rapid changes in water pressure which affects the turbine surface. Hydro corrosion problems are associated with damaging particles [8]. In November 1995, a special 204 MW Kaplan turbine was commissioned at the hydroelectric plant. Shuikou in China on February 10, 2000, the turbine suffered severe vibrations and the oil level dropped significantly. From inspection the central exhaust pipe of the piston rod broke, leading to outstanding investigations [8].

Figure 1.1: Fractured piston rod a. nut structure b. retainer ring structure [8].

The initial structure of the nut was replaced with mounting rings, but failed in the same manner on March 16, 2006. Dynamic analysis revealed problems with the project. It addresses failure due to fatigue caused by sudden pressure on the runner blade, from fluid to mechanical energy under enormous hydraulic pressure [8]. In another Romanian case study, a 35.5 MW hydro Kaplan turbine rotor in Romania suffers fatigue failure In particular, turbines of cascade hydropower plants operate at higher manometric heights. The investigation revealed that the cracks were caused by the concentration of pressure between the foot and the flange in the direction of the attack edge as revealed by metallurgical observations and calculations [12].

Figure 1.2 the cracked runner blade of a 35.5 MW kaplan turbin in Romania[12]

1.2 Statement of the problem

The Kaplan hydraulic turbine is broadly utilized in hydroelectric power technology because of its performance in managing variable water flows. However, the performance and longevity of its components, particularly the runner blades, are severely influenced by way of fatigue and fracture mechanisms. The complex loading situations and material fatigue experienced through those blades throughout operation can lead to premature failure, resulting in vast (significant) downtime and economic losses. [41]

One's a defect happens inside the material, it may be regarded as an initiated crack. Over time, this crack can grow to a crucial size due to fatigue propagation, that's influenced by means of a specific wide variety of load cycles, ultimately leading to the fracture of the blade. This thesis normally aims to recognize the behavior and characteristics of cracks initiated by using fatigue loads, that is crucial for comprehending how those cracks propagate and for estimating the fatigue life of Kaplan turbine runner blades. This knowledge is essential for preventing further damage as a consequence of the separation of the runner blade from its root. This research targets to address with the gap by means of developing a numerical model to analyze the fatigue growth rate and fracture life of Kaplan turbine runner blades.

1.3 Objectives Of the Thesis

1.3.1 General Objective

The over all objective of this thesis is Numerical investigation of fatigue growth rate and fracture lifetime estimation of Kaplan hydraulic turbine runner blade.

1.3.2 Specific Objective

- To investigate the fatigue crack propagation on the Kaplan hydraulic turbine runner blade with fatigue load.
- To estimate the fracture lifetime of Kaplan turbine runner blades based on the numerical results of fatigue growth.
- To discuss ANSYS result and interpret the Results.

1.4. Research Methods and methodology

1.4.1 Methods

A. Literature review

A literature review involves searching for articles that show similar work done in the past. This means about investigation of fatigue crack growth rate and facture life estimation of Kaplan hydraulic turbine runner blade. If I say this, the basis of literature review will be appropriate literature articles from journals, internet and books. After that, I will write secondary data from research papers that have been done before, statistical data that have been written, you tube video and so on.

B. Data collection

In order to analyze Kaplan hydraulic runner blade geometrical specifications and loading conditions data, I will design small Kaplan turbine runner blade using appropriate design manual.

C. Modeling and simulation of Kaplan runner blade

- Using numerical method for analysis.
- Making airfoil shape using MATLAB
- Making 3D design model using solid work software, performing simulation for the model using ANSYS workbench 2020R1 software.

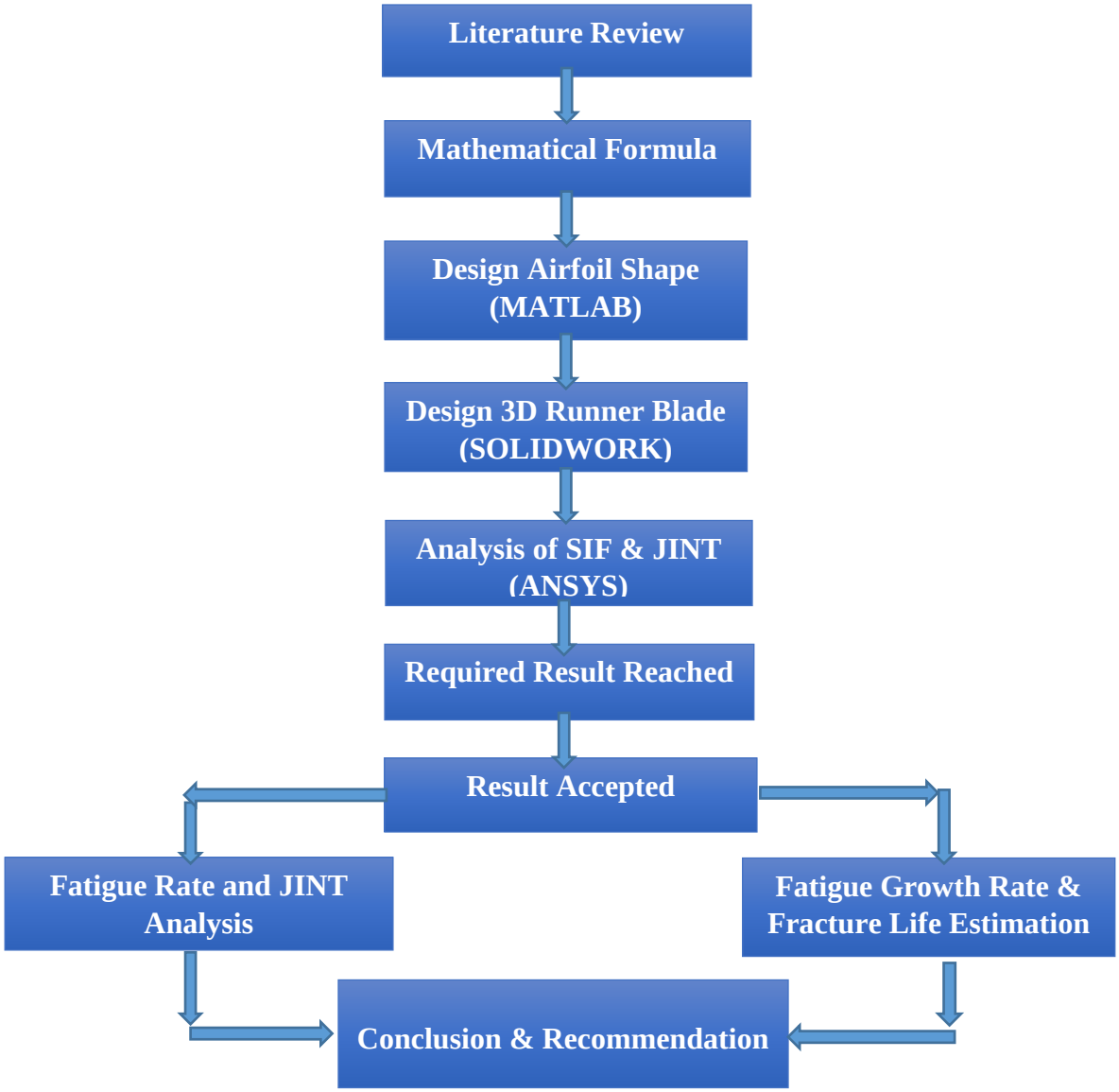

Figure 1.3 design, fatigue and fracture analysis methods Flow chart

Figure 1.3 indicates the general design, fatigue and fracture analysis methods chart of runner blade. The process started with reviewing related literature to the hydro Kaplan turbine runner blade. The mathematical formulas were used for the designing of Kaplan runner blade. The obtained result is converted into airfoil shape using MATLAB software. Next by directly taking the matlab analysis result to SOLIDWORK, a 3D model is obtained, and then using ANSYS software stress intensity factor and J-integral result are obtained. After obtaining the desired result fatigue growth rate and fracture life will be estimated. When the requested conditions were fulfilled, write the conclusion and recommendation.

1.5 Scope and limitation of the study

The scope of this thesis is numerically investigate the fatigue growth rate and estimated the fracture life of Kaplan hydraulic turbine blades with the help of ANSYS software framework. The cause of crack initiation is due to fatigue load, Cavitation and corrosion. While the cause of crack propagation is due to the material being stressed or deformed by residual stress or direct application of stress or strain.

The study only focuses on numerical investigation of the fatigue growth rate and estimate the fracture life of Kaplan hydraulic turbine runner blades due to fatigue load case. Experimental test is not performed in this study. Due to the broad scope of environmental impacts, other loading situations aren't addressed like corrosion, vibration of the runner blade, wear problem, cavitation, creep results, the effect of surface finish on the material and thermal load on this paper.

1.6 Significance of the study

This studies will enhance the know-how of fracture mechanics, particularly within the vicinity of fatigue crack propagation. It will mainly advantage technicians concerned in the layout, production, and maintenance of hydroelectric power plant the usage of hydro Kaplan runner blade. The findings will contribute precious insights into the fatigue crack propagation traits of hydro Kaplan runner blade and help estimate their fatigue lifestyles as soon as a crack initiates. Given the high expensive of experimental methods, utilizing FEM evaluation software for modeling and simulation will provide a price-powerful opportunity, permitting quicker effects and reducing the need for sizeable bodily checking out.

1.7 Outlines of the thesis

This section explains the structure of the thesis and briefly summarizes each chapter. It helps the reader understand how these things are organized and what to expect from each part.

Chapter One: Introduces the research and explains its objectives. It provides a general historical overview of the research and its significance. This is followed by the objectives, methodology, and scope of the research. At the end of the chapter the organization of these is explained, along with a brief description of the following chapters.

Chapter Two: This is a literature review that examines several studies related to fatigue growth rate and Kaplan's estimation of the fracture life of turbine blades. Related research carried out by

various academics is analyzed. Summary of findings, recommendations, and conclusions on the topic.

Chapter Three: Describe the Kaplan turbine blade design process and develop equations to estimate fatigue growth rate and blade life. Covers important concepts in fluid dynamics and solid mechanics that affect blade performance. This chapter also includes a brief overview of the methods for calculating the main dimensions of blade and their development using the relevant empirical formulas. This section discusses the basic principles and calculations required to understand and operate a Kaplan turbine rotor blade.

Chapter Four: provides detailed instructions on how to use ANSYS to analyze a 3D model of a Kaplan turbine rotor. It describes the ANSYS Workbench steps for sheet analysis. This includes geometric modeling, mesh generation, and loading configuration and conditions of shape. This chapter discusses how to prepare models for analysis, Run the simulation and interpret the main results.

Chapter Five: presents the results of the ANSYS Workbench software, tabulating various parameters that is calculated by adding the crack length and show relationships through numbers.

Chapter Six: provides conclusions drawn from the results and makes recommendations based on the conclusions.

Chapter Two

2. Literature Review

2.1 Fracture mechanism of fatigue growth rate

This chapter is a literature review focusing on fatigue growth rate and estimation of the fracture life of Kaplan hydroelectric turbine blades. Various studies and research will be discussed briefly related to this topic. This chapter analyzes the findings, recommendations, and conclusions of various researchers. It highlights contributions and insights into the two Kaplan turbine runner blade. Many studies have been conducted to analyze the fatigue life of two Kaplan turbine blades, especially in developing countries where hydroelectric power is the main energy source. Several methods and approaches have been used to investigate fatigue behavior in different countries. The goal is to improve performance and longevity. Researchers use a variety of techniques including numerical simulation, experimental test and analysis methods to understand how fatigue affects both under operational conditions. As a result, many studies have been published that provide valuable information about the sustainability of countries and the mechanisms of failure. The following paragraphs analyze some of this research. It summarizes the research results and highlights the progress in analyzing and solving the fatigue problem in the Kaplan turbine blades.

Waleed, K.M., Reza Kashyzadeh, K. and Ghorbani, S. [9] Survey of prominent defects in Kaplan turbines used in low residual water hydropower plants. They emphasize the economic impact of these deficiencies and emphasize the importance of understanding their causes. We present a prevention strategy and outline future research directions, focusing on a blade failure in Iraq.

Johnson and Patel (2023). [14] Johnson and Patel performed a detailed review of fatigue growth rate models specific to Kaplan turbine runner blade spacing. They focused on using principles of fracture mechanics to predict crack propagation that reduces typical cyclic loading conditions in hydroelectric turbines. This review discusses various models of crack growth due to fatigue including Paris laws and turbine blade modifications and how do these models help estimate the fracture life of blades under operating stress.

Khalid, W.M.R., Kashyzadeh, K.R. and Ghorbani, S., 2024. [27] Investigated failure in Kaplan turbines, focusing on blade faults in Iraqi hydroelectric plants. They emphasize the importance of understanding the causes of failure to mitigate economic losses associated with repairs. From

various tests including quantitative inspection and metallurgical examination. They found that the blade was made of 304 stainless steel with extensive damage due to severe cavitation. The authors outline future research directions to develop fault detection and prevention strategies in Kaplan turbine systems, providing valuable insights to improve long-term performance and reliability in hydroelectric applications.

Valid, H.M.R. , Kazem, R.K.Z. and Siamak, G (2024).[20] Investigating defects in Kaplan turbines, focusing on blade defects in Iraqi hydroelectric plants. We emphasize the economic impact of these errors and the need for effective detection and prevention strategies. His open testing revealed that the runner blade made from 304 stainless steel had suffered severe cavitation damage. The study emphasizes the importance of understanding failure mechanisms to improve turbine design and service life, this leads to future research to improve the reliability of hydropower systems.

Brown and Wang (2023). [11] Brown and Wang investigated the effect of hydrodynamic load variations on the fatigue life of Kaplan turbine rotor sides. This review discusses several stress analysis methods includes finite element modeling and analysis techniques. To consider stress concentration and material degradation. It provides insight into how operational loading conditions affect crack growth rate and blade durability.

Ubulom, I (2019) [24] They emphasize the importance of accurately modeling these interactions to predict their performance under operational conditions. The authors used advanced computational methods to simulate the effects of fluid dynamics and thermal load on pavement integrity. These findings reveal important insights into stress distribution and where defects may occur, this improves our understanding of fatigue mechanisms.

Liu, X., Presas, A., Luo, Y. and Wang, Z., 2018 [15] apply linear elastic fracture mechanics (LEFM) to investigate fatigue issues in a major Kaplan hydraulic turbine, where repeated failures of the piston rod occurred. They simulated crack growth using the LEFM technique, combining a probabilistic model for the initial crack size. Reliability analysis focuses on the relationship between initial rupture conditions and operational factors. It provides insight into the likelihood of a critical fracture occurring. The predicted crack path and loading cycle are consistent with observed fracture zones. This demonstrates the potential of LEFM to improve fatigue analysis in turbo hydraulic machines.

Garcia and Miller (2015). [23] Garcia and Miller provide a review of two failure modes associated with fatigue of Kaplan turbines. They discuss the widening of different types of crack propagation and the impact on the integrity of the blade. It emphasizes the importance of complete failure analysis for accurate service life estimation and maintenance planning.

Roig, Rafel, et al. [10] In their study investigated fatigue damage in Kaplan turbine blades under non-design transient conditions including the speed-no-load (SNL) and part-loading (PL) speeds, they found that the SNL operation caused sudden flow shocks causes more damage. While PL damage is related to the rotating vortex. Their research highlights the importance of sensor data for accurate estimation of blade fatigue.

Smith and Brown (2016). [19] Review of Smith and Brown's methods for predicting the fracture life of Kaplan turbine blades, focusing on probabilistic approaches. It discusses the use of statistical models to estimate the probability of propeller failure over time and reliability analysis including uncertainties in material properties and loading conditions.

Huth, H.J., Doctoral thesis 2005. [13] Investigation of hydraulic turbine blade fatigue project. Depends on start-stop cycle and vibration. They point out that crack objects resulting from service or manufacturing defects can become critical when vibration forces exceed fatigue limits. The authors focused on the semi-elliptical surface of the crack in a welded T joint, using finite element analysis to model the stress field. They show that micro crack growth is minimally influenced by the geometry makes it easier to predict.

Moraga, G., Mut, V., Girardelo, J., Mazzouji, F., Valentín, D., Egusquiza, M., Egusquiza, E. and Presas, A., 2024. [21] study on excessive vibration at Kaplan turbine head at no load speed. Preliminary analysis suggests that blade resonance is the source of the problem, Especially in covering the head. Despite the changes in the roots of blade but the level of vibration continued to increase, as a result the commissioning test was delayed. To identify problems the authors installed a series of sensors and performed an experimental analysis of the runner head coverage. His opening tests revealed the vibration transmission path of the runner blade steps.

Moreover, Li et al.'s (2019) research used advanced principles of fracture mechanics to develop a predictive model to estimate fracture lifetime based on crack growth rate and material properties.

These findings highlight the importance of considering environmental factors such as temperature and water pressure to estimate the fracture life.

To identify the causes that lead to propeller failure. The researchers carried out metallurgical investigations using a scanning electron microscope (SEM) on the blade's resistance and lifespan assessment. During the investigation high content of non-metallic inclusions in the blade material happened in position 1. The water used takes into account the corrosion of the surrounding base material. As a result the non-metallic inclusions released from the surface leaving creaters behined position 2, Which were filled in with corrossion products postion 3. Finally, on the surface of the examined sample. Many secondary grooves were also observed, especially at the 4th position of the crack by fatigue [12].

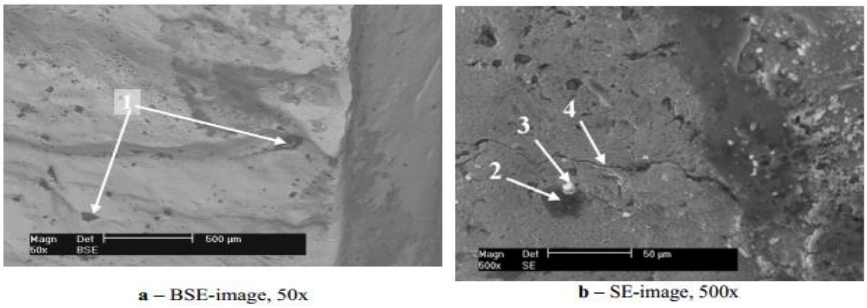

a – BSE-image, 50x **b** – SE-image, 500x

Figure 2.1 micrographs of the fracture surface of kaplan turbine runner blade [12]

Ming Zhang , David Valentín , Carme Valero, Mònica Egusquiza and Eduard Egusquiza, address a rare failure mode of Kaplan turbine blades, characterized by a significant crack originating from the leading-edge root hole and a broken blade tip. The investigation was prompted by a sudden spike in vibration levels detected by the turbine's monitoring system. Initial inspection confirmed the presence of the crack and additional damage to the blade tip, indicating a severe mechanical issue. A thorough examination of the crack surfaces, broken components, and vibration data suggested a fatigue failure, likely caused by rubbing between the blade and an adjacent wall [41].

To understand the impact of contact forces on stress distribution within the blade, the authors developed a numerical model. This model was validated through experimental modal analysis conducted on an undamaged blade, showing strong correlation with the numerical predictions. The stress distribution analysis revealed that contact forces significantly increased stress at the leading-edge root hole [41].

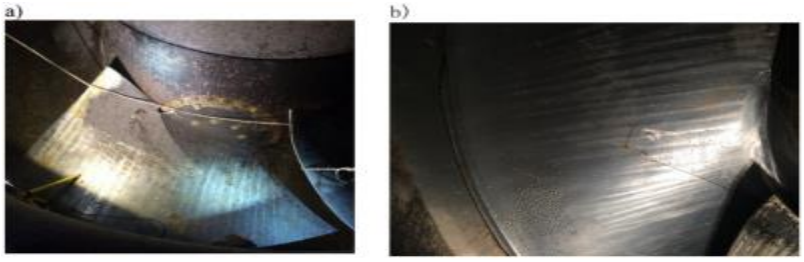

Figure 2.2a pressure side Figure 2.2b suction side

Figure 2.2 View of blade with crack [41]

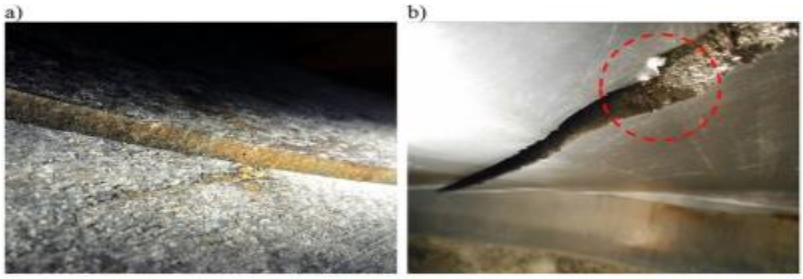

Figure 2.3a From the pressure side. Figure 2.3b From the suction side.

Figure 2.3 Details of the crack [41]

Both experimental observations and numerical simulations collectively support the conclusion that the blade failure was due to rubbing between the blade tip and the nearby wall. This investigation highlights the importance of monitoring and analyzing mechanical stresses in turbine blades to prevent similar failures and ensure the reliable operation of Kaplan turbines. The integration of experimental and numerical approaches provides a comprehensive understanding of the failure mechanism and offers valuable insights for future design and maintenance strategies.

2.2 Stage of Fatigue failure for critically loaded component

Murakami, Fatigue is accountable for 80-90% of fractures, predominantly happens at geometric irregularities like holes, notches, and transitions. Cracks initiate at areas with the very best neighborhood pressure, frequently near notches. Initial flaws, including cracks and macro-notches, intensify stress concentration, impacting the structural integrity. A severely loaded element's crack lifecycle involves 5stage: initiation, brief propagation (microstructurally and mechanically/physically), protracted propagation, main to final structural fracture in fatigue failure.

Fatigue failure in critically loaded components typically progresses through several distinct stages:

1. **Crack nucleation:** This preliminary degree involves the formation of microscopic cracks at regions of high stress attention, including surface defects, inclusions, or irregularities. These small cracks broaden due to cyclic loading and strain versions.
2. **Crack Propagation:** Once nucleated, the cracks begin to grow with every load cycle. This degree is characterized by using the gradual extension of cracks through the material. The growth rate can vary depending on the material properties, loading situations, and environmental elements. This degree is often analyzed the usage of Paris' Law, which relates the price of crack growth to the range of strain intensity thing.
3. **Final Fracture:** In the final stage, the crack reaches a crucial size where the final material cannot withstand the applied loads. The crack rapidly propagates, leading to a catastrophic failure of the aspect. This stage is marked by way of a surprising and frequently entire breakage of the factor [16].

2.3 Fracture Life

Fatigue and fracture growth over the life cycle of hydraulic Kaplan turbine blades are important in evaluating reliability and performance. The literature indicates that the aging life of these components is typically in the range of $5x10^7$ to $2x10^8$ cycles, which is affected by physical properties and operating stresses. Fatigue crack growth rate it typically decreases between 10^{-6} and 10^{-6} mm/cycle, depending on the stress intensity factor experienced during operation [44].

Dorian Nedelcu, Viorel Constantin Câmpian, and Ioan Pădurean: Investigated the service existence estimation for the runner blades of an axial turbine. Literature shows that fatigue life estimates for those components display that risky fissures seem after 10^{10} fatigue cycles (approximately 60,000 running hours) at the trailing edge, while at the leading edge, dangerous fissures seem after 10^9fatigue cycles (approximately 10,000 operating hours)[12].

Smith & Turner(2018): Studied fracture existence cycles for Kaplan turbine blades typically exceed $5x10^8$ cycles, with some research reporting values as high as $2x\ 10^9$ cycles .This extensive sturdiness highlights the blades' ability to face up to prolonged cyclic loading without catastrophic failure[45].

2.4 Research gap

The lack of both elastic and plastic fracture approaches for analyzing Kaplan turbine runner blades under fatigue loading complicates the assessment of their structural integrity. Fatigue loads, caused by cyclic stresses during operation, lead to micro crack formation and eventual failure. Elastic fracture mechanics typically addresses initial crack propagation, while plastic fracture mechanics considers the material's permanent deformation under stress.

Without integrating both approaches, analyses overlook critical failure mechanisms, such as the transition from elastic behavior to plastic deformation as fatigue progresses. This gap results in inaccurate predictions of the blade's lifespan and failure modes. Consequently, engineers struggle to optimize blade design for enhanced durability and safety. To improve reliability, it is essential to develop comprehensive models that incorporate both elastic and plastic fracture mechanics, enabling a better understanding of how Kaplan turbine blades respond to fatigue over time.

2.5 Material selection for hydro Kaplan turbine runner blade

Researchers conducted various studies to identify optimal materials for hydropower plant turbines. Due to diverse loads and environmental conditions, finding the right material properties posed a challenge. To address this, different materials are employed for specific components of the turbine, enhancing overall efficiency and durability.

Among all stainless steel, since 304 stainless steel have a lot of chromium and nickel, they are very resistant to destructive phenomenon such as erosion, wear and corrosion. This is why they are widely used to manufacture blades for hydro turbines [8].

Table 2.1 Chemical Composition of Stainless steel 304 (SS 304) [17]

Element	C	Cr	Ni	Si	Mn	P	S	N
Wt.%	0.07	18.0–19.5	8.0-10.5	1.00	2.00	0.045	0.015	0.10

Table 2.2 Material properties of Stainless steel 304 (SS 304) [17]

Properties(SS 304)	**Value**
Density	8 g/cm^3
Modulus of elasticity	193 Gpa
Thermal conductivity	16.2 W/m.k
Shear Modulus	77 Gpa
Ultimate tensile strength	505 Mpa
Tensile Yield Strength	215 Mpa
Hardness(Rockwell B)	70
Elongation at break	70 %
Poisson's Ratio	0.33
Melting point	1450 C^o
Electrical Resisting	0.72 x 10.6 ohm
Fatigue Strength	+ or - 400
Plain strain fracture toughness(K_{IC})	283 KJ/m^2

Shear strength = 0.60 x Ultimate tensile strength and Shear strength = 0.60 x 505 Mpa =303 Mpa

Chapter Three

3. Fracture Mechanics Approach and Designing of the runner blade

3.1 Basics of Fracture mechanics

Fracture mechanics focuses on knowledge how cracks have an effect on the mechanical conduct of deformable materials. It goals to explain and degree a material's resistance to crack increase, studying how those defects effect normal energy and integrity [30]. Fracture mechanics is a vital discipline of study inside materials technology and engineering that examines the conduct of substances containing cracks or flaws. This subject focuses on information how those imperfections have an effect on the mechanical properties and overall performance of materials under diverse strain situations. By analyzing the initiation and propagation of cracks, fracture mechanics helps in predicting and preventing catastrophic failures in systems and components. This understanding is critical for designing more dependable materials and engineering structures, making sure protection, and enhancing the longevity of crucial infrastructure. Fracture mechanics integrates principles from mechanics, materials technological know-how, and mathematics to cope with challenges associated with material durability and structural integrity.

3.2 Purpose of Fracture mechanics

In simple phrases, whilst a shape undergoes repeated pressure, it might develop a fatigue crack. As this crack gets longer, it creates extra pressure in that region, causing the crack to spread quicker. This weakens the structure. Eventually, the structure won't be strong enough to handle the best loads it faces, risking failure. As the crack continues growing, the structure's strength decreases until it can't handle even normal masses, making failure probable [12].

- The residual strength as a feature of crack size
- The crack length that can be allowed at the anticipated carrier load (the important size)
- How long it takes the crack to develop from a positive size to a vital size
- The size if preliminary flaws that can be tolerated in a new issue
- The interval between inspections for cracks

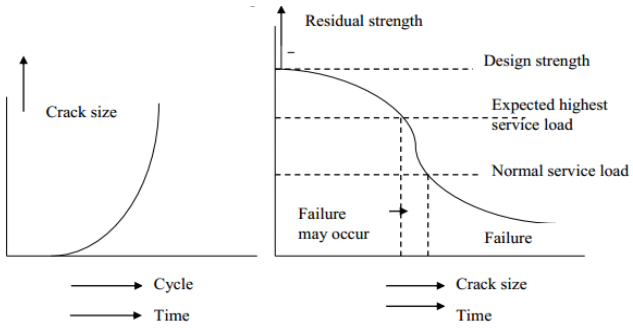

Figure 3.1 Relationship between crack length and failure load

3.3 Fracture parameter and stress intensity factor

Fracture behavior is normally defined using 3 or 4 key parameters. For elastic substances, the number one parameters are the strain intensity factor and the energy release rate. These metrics help quantify how cracks have an impact on the material energy (strength) and how they propagate under pressure. For elastoplastic substances, the J-integral and the crack tip opening displacement are used to signify fracture. These parameters offer insights into how materials with greater complicated behavior, including plastic deformation, respond to cracking [18].

In ANSYS, a broadly used engineering simulation software, cracks are modeled the usage of those parameters: pressure depth issue, energy release rate, or the J-integral. The preference of parameters relies upon at the kind of material and loading situations concerned. By utilizing those parameters, ANSYS can correctly simulate and analyze crack behavior, assisting engineers expecting material overall performance and prevent failure in diverse structural programs.

3.3.1 Stress Intensity Factor

The stress intensity factor, KI, plays a critical position in fracture mechanics through quantifying the intensity of stress near the tip of a great crack in linear elastic materials. It is critical for predicting how cracks propagate under external loads or residual stresses. This parameter, specific to homogeneous elastic materials, serves as essential tool in establishing failure criteria for brittle substances. For ductile substances, fracture behavior is normally assessed the usage of opportunity parameters consisting of the J-critical or crack tip opening displacement. These measures offer insights into the power release charge and deformation techniques near the crack tip, imparting a complete understanding of fracture resistance and durability in materials liable to plastic deformation.

The value of KI is influenced by means of sample geometry, crack size and region, and the distribution of loads on the material. Various techniques exist to calculate stress depth elements as it should be. They may be categorized as

1. Theoretical (Wastergaard semi-inverse approach and method of complicated potentials).
2. Numerical (Green's characteristic, weight functions, boundary collocation, alternating approach, imperative transforms, non-stop dislocations and finite elements methods).
3. Experimental (photograph elasticity, moiré, holography, caustics, and combinations of these strategies).

Theoretical methods are constrained to infinite plates with easy crack geometries and boundary situations. Complex eventualities require numerical or experimental methods for accurate evaluation.

3.3.2 Mode of Fracture

In structures with cracks, the force or stress near the tips of the cracks can cause three types of fractures. These fractures are called modes, and they are shown in the figure below. The three modes are categorized as [18].

A. Mode one failure(mode I loading) or tension failure :It is an Opening mode where the crack surfaces separate symmetrically with respect to the plane occupied by the crack prior to the deformation (results from normal stresses perpendicular to the crack plane);

Figure 3.2 Mode I or opening mode [18]

B. Mode two failure(mode II loading): It is sliding mode where the crack surfaces slide over one another in opposite directions but in the same plane (results from in-plane shear).

Figure 3.3 Mode II or sliding mode [18]

C. Mode three failure(mode III loading): It is tearing mode where the crack surfaces are displaced in the crack plane and parallel to the crack front (results from out-of-plane shear)

Figure 3.4 Mode III or tearing mode [18]

3.3.3 Linear-Elastic fracture mechanics parameter

In linear-elastic fracture mechanics (LEFM), the primary parameters used to explain and analyze crack behavior in substances are:

Stress Intensity Factor (SIF) This parameter quantifies the intensity of the pressure area close to the crack tip. It is important for predicting the chance of crack propagation beneath diverse loading situations. The pressure depth factor depends on the kind of loading (tensile, shear, or bending) and the crack geometry.

Energy Release Rate (G): This parameter measures the intensity at which elastic strain electricity is released from the material as a crack grows. It offers insight into the driving force behind crack propagation. The energy release rate is often used to determine the crucial value at which a crack will grow, called the fracture toughness (Gc).

Fracture Toughness (Kc): This is a material belongings that represents the critical stress intensity thing at which crack increase occurs. It is a measure of a material resistance to fracture and is used to evaluate whether or not a material can withstand the presence of cracks under given loading situations.

Critical Stress Intensity Factor (SIFc): This is the maximum strain intensity aspect a material can resist before crack propagation initiates. It is a key parameter in determining out the materials fracture durability and assessing its overall performance in structural applications.

These parameters are essential for comparing the structural integrity of substances and predicting failure in engineering applications.

3.3.4 Elastic-plastic fracture mechanics parameter

3.3.4.1 Crack-tip opening displacement

The crack tip opening-displacement(CTOD) was firstly introduced by wells(1961) in the attempt to quantify the fracture toughness of a number of structural steels that he found too tough to be characterized by LEFM.

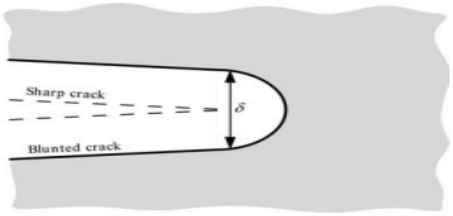

Figure 3.5 Initially sharp crack blunts with plastic deformation [18]

An initially sharp crack blunts with plastic deformation, resulting in a finite displacement δ at the crack tip.

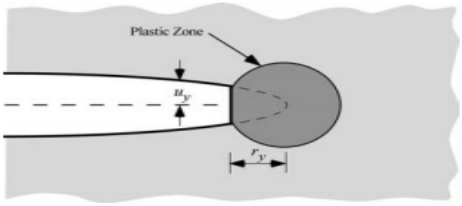

Figure 3.6 displacement of crack tip along Y-axis [18]

The displacement of crack tip along Y-axis(and on the crack plan) is given by:

$v = \frac{K_I}{E}\sqrt{\frac{r}{2\pi}}$ plane stress condition and on the crack plane at $\theta = \pi$

In the limit of small scale yilding, wells performed an appropriate analysis that related CTOD to the stress intensity factor:

$$\delta = 2v = \frac{8K_I}{E}\sqrt{\frac{1}{2\pi}\frac{1}{2\pi}\left(\frac{K_I}{\sigma_{ys}}\right)^2} = \frac{4}{\pi}\frac{{K_I}^2}{\sigma_{ys}E} \qquad (3.1)$$

The crack-tip opening displacement(CTOD) is a crucial parameter in fracture mechanics, indicating the size of the crack opening at the tip of a crack in a material subjected to loading. For a kaplan turbine blade, which operates in a high-stress environment due to fluid flow, underestanding CTOD is essential for predicting and preventing crack propagation.

The equation governing CTOD typically involves factors such as the applied stress, crack geometry, and material properties. A common expression for CTOD under certain conditions is given by the Irwin or crack opening displacement formula.

$$r_y = \frac{1}{2\pi}\left(\frac{K_I}{\sigma_{ys}}\right)^2 \text{ Irwin approach} \qquad (3.2)$$

Alternatively, CTOD can be related with to the energy release rate as given by: $\delta = \frac{4}{\pi}\frac{G}{\sigma_{ys}}$

According to the strip yield model(Dugdale Approach)-plastic zone size of crack tip in an infinite plane was determined by considering closure stress which equivalent with yield strength.

They assume: long slender plastic zone in a nonhardning material in plastic stress(ρ)

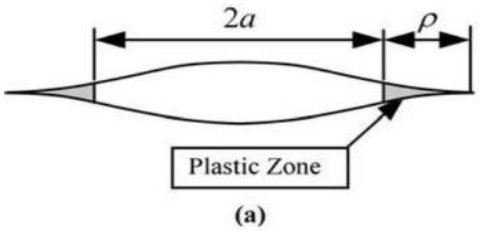

Figure 3.7 crack in an infinite plane subjected to the remote tensile stress , σ[18]

Through crack in an infinite plane subjected to the remote tensile stress , σ.

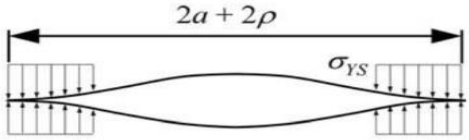

(b)

Figure 3.8 crack in an infinite plane subjected to compressive(closure) stress [18]

Through crack in an infinite plane subjected to compressive(closure) stress.

We can evaluate plastic zone size and effective stress intensity factor simply from balancing stress intensification determined from remote stress and compressive stress.

$$\rho = \frac{\pi^2\sigma^2 a}{8_{\sigma_{ys}{}^2}} = \frac{\pi}{8}\left(\frac{K_I}{\sigma_{ys}}\right)^2 \quad \text{plastic zone size} \qquad (3.3)$$

$$K_{eff} = \sqrt[\sigma]{\pi a \, sec\left(\frac{\pi\sigma}{2\sigma_{ys}}\right)} \quad \text{Effective stress intensity factor} \qquad (3.4)$$

3.3.4.2 J-contour integral

J-Rice obtained a path independent contour integral called J which is given by:

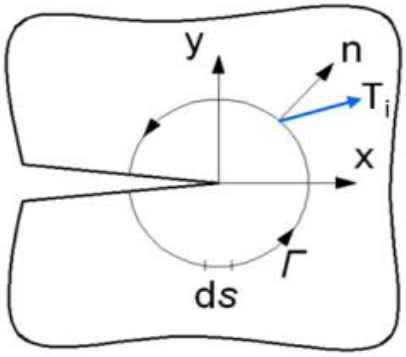

Figure 3.9 path independent contour integral [18, 43]

$$J = \int_{\Gamma}^{0}\left(W dx_2 - T_i \frac{\partial U_i}{\partial X_1}\, ds\right) \quad (\text{i= 1, 2}) \qquad (3.5)$$

$$W = \int_0^{\varepsilon_{ij}} \sigma_{ij}\, d\varepsilon_{ij} \quad \text{linear or non-linear elastic material behavior}$$

$$T_i = \sigma_{ij} n_i$$

Where: Γ - is an arbitrary curve around the tip of a crack

W- is the strain energy density

T_i – is the component of the traction vector

u_i – is the displacement vector components

ds – is the length increment along the contuor

x and y – are the rectangular coordinates with the y direction taken normal to the crack line and the origion at the crack tip.

3.3.4.3 Relationship between J-integral and potential energy

In an elastic solid the potential energy Π is given by:

$\Pi = U - F$ where: U strain energy F external work done

$U_T = U - U_C$ where: U_T Total strain energy U Strain energy with out rack U_C strain energy due to crack (3.6)

And it is related to the strain energy release rate by the relationship:

$$G = \frac{dU}{dA} - \frac{dF}{dA} = -\frac{d\Pi}{dA} \text{ .....Griffith energy balance} \quad (3.7)$$

It can be also shown that for nonlinear elastic materials for any path of integration surrounding the crack tip:

$$J = \int_{\Gamma}^{0} \left(W dx_2 - T_i \frac{\partial U_i}{\partial X_1} ds \right) = -\frac{\partial \Pi}{\partial A}$$ For linear elastic material: J=G (3.8)

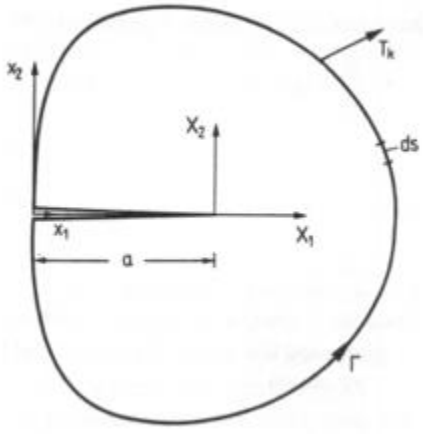

Figure 3.10 A two dimensional cracked body

3.4 Fundamental equations of fluid mechanics

For the analysis of incompressible fluid flow through Kaplan hydraulic turbine blades, the governing equations normally consist of the continuity equation and the Navier-Stokes equations. These equations describe the conservation of mass and momentum, respectively, in the fluid flow. In addition to these, the power equation also can be covered to account for changes in strength within the flow.

3.4.1 Conservation of mass

The conservation of mass, expressed through the continuity equation, is a essential principle in fluid mechanics that states the entire mass coming into a control quantity should same the total mass leaving the control quantity, plus any mass accumulation in the volume. For Kaplan hydraulic turbine blades, this principle is critical for information the flow of water through the turbine.

Consider a manipulate extent V with a surface area S through which the fluid flows. The mass of the fluid on this manipulate volume at time t is:

$$m(t) = \int_V^0 \rho(X,t)dV \tag{3.9}$$

Where $\rho(X,t)$ is the density of fluid at position X and time t

The rate of change of mass inside the control volume is:

$$\frac{d}{dt}\left(\int_V^0 \rho dV\right) \tag{3.10}$$

By applying the Leibniz rule for differentiation under the integral sign:

$$\frac{d}{dt}\left(\int_V^0 \rho dV\right) = \int_V^0 \frac{\partial \rho}{\partial t} dV \tag{3.11}$$

The flux of mass through the surface S is given by:

$$\text{Flux} = \int_S^0 \rho v.ndS \tag{3.12}$$

where n is the outward unit normal to the surface S. According to the Divergence Theorem, this surface integral can be converted into a volume integral:

$$\int_V^0 \rho v.ndS = \int_V^0 \nabla.(\rho v)dV \tag{3.13}$$

For the mass to be conserved, the rate of change of mass within the control volume must be equal to the negative of the net flux of mass out of the control volume:

$$\frac{d}{dt}\left(\int_V^0 \rho dV\right) + \int_S^0 \rho v.ndS = 0 \qquad (3.14)$$

Substitute the expressions for the rate of change of mass and the net flux through the surface:

$$\int_V^0 \frac{\partial \rho}{\partial t} dV + \int_V^0 \nabla.(\rho v) dV = 0 \qquad (3.15)$$

Since this must be true for any arbitrary control volume V, the integrands themselves must be equal. Thus, we have:

$$\boldsymbol{\frac{\partial \rho}{\partial t} + \nabla.(\rho v) = 0} \qquad (3.16)$$

where: ρ fluid density v velocity vector field

t time, ∇ divergence operator

For steady, incompressible flow (which is often assumed in Kaplan turbine analysis), the continuity equation simplifies to:

$$\nabla.v = 0$$

This equation states that the divergence of the velocity field is zero, indicating that the flow is steady and there is no net change in mass within the control volume.

3.4.2 Conservation of momentum

The conservation of momentum is another fundamental principle in fluid mechanics that governs the motion of fluids, including the flow through Kaplan hydraulic turbine blades. The conservation of momentum is expressed through the Navier-Stokes equations, which describe the motion of fluid particles within a flow field.

Newton's second law states that the rate of change of momentum of a fluid element is equal to the sum of the forces acting on it.

For a fluid element of density ρ and velocity , the momentum is ρV. Thus, the rate of change of momentum for a fluid element is:

$$\frac{D(\rho v)}{Dt} = \frac{\partial(\rho v)}{\partial t} + v.\nabla(\rho v) \quad (3.17)$$

Where $\frac{D}{Dt}$ is the material derivative, accounting for both local and convective changes in momentum.

First, let's expand the term $\frac{\partial(\rho v)}{\partial t}$:

$$\frac{\partial(\rho v)}{\partial t} = \rho\frac{\partial v}{\partial t} + v\frac{\partial \rho}{\partial t} \quad (3.18)$$

For an incompressible fluid, $\frac{\partial \rho}{\partial t} = -v.\nabla\rho$ Thus:

$$\frac{\partial(\rho v)}{\partial t} = \rho\frac{\partial v}{\partial t} \quad (3.19)$$

The convective term $v.\nabla(\rho v)$ can be expanded using the product rule:

$$v.\nabla(\rho v) = \rho(v.\nabla \mathrm{v}) + v(v.\nabla\rho) \quad (3.20)$$

For an incompressible fluid, $\nabla.\mathrm{v} = 0$, so $v.\nabla\rho = -\rho(\nabla.\mathrm{v}) = 0$ Therefore:

$$v.\nabla(\rho v) = \rho(v.\nabla \mathrm{v}) \quad (3.21)$$

Combining the terms, the total rate of change of momentum is:

$$\frac{D(\rho v)}{Dt} = \frac{\partial(\rho v)}{\partial t} + \rho(v.\nabla \mathrm{v}) \quad (3.22)$$

The forces acting on the fluid element include:

- **Pressure Forces:** The pressure P exerts a force $-\nabla\rho$ per unit volume. Thus, the force per unit volume is $-\nabla P$.
- **Viscous Forces:** The viscous forces can be represented by the term $\mu\nabla^2 v$, where μ is the dynamic viscosity of the fluid.
- **Body Forces:** Body forces, such as gravity, act on the fluid. If g is the acceleration due to gravity, the body force per unit volume is ρg.

For an incompressible flow of Newtonian fluid (which is often assumed in Kaplan turbine analysis), the Navier-Stokes equations can be simplified to:

$$\boldsymbol{\rho\left(\frac{\partial v}{\partial t}+v.\nabla v\right)=-\nabla p+\mu\nabla^2 v+\rho g} \quad (3.23)$$

Where: ρ fluid density v velocity vector field μ dynamic viscosity of the fluid
t time p pressure g acceleration due to gravity

3.4.3 Conservation of energy

The conservation of energy is a fundamental principle in fluid mechanics that governs the transfer and transformation of energy within a fluid float. In the context of Kaplan hydraulic turbine blades, the conservation of strength is critical for know-how the energy conversion process from the kinetic strength of flowing water to mechanical power inside the turbine rotor.

The conservation of energy in fluid mechanics is commonly expressed through the electricity equation, which account for adjustments in internal strength, kinetic strength, and potential strength within the fluid flow. The power equation can be written in numerous forms depending on the precise conditions of flow, together with whether it includes compressible or incompressible go with the flow, constant-state temporary flow, and the presence of heat transfer or viscous dissipation.

For the flow of incompressible fluid (which is regularly assumed in Kaplan turbine analysis) without heat transfer, the electricity equation can be simplified to:

The total energy per unit mass E of the fluid consists of:

- **Internal Energy per Unit Mass (e)**: The energy associated with the fluid's thermodynamic state.
- **Kinetic Energy per Unit Mass**:$\frac{1}{2}v.v$, where $v.v$ is the squared magnitude of the velocity.

Thus:

$$E=e+\frac{1}{2}v.v \quad (3.24)$$

Consider a control volume with density ρ. The total energy within the control volume is:

$$Total\ energy=\int_V^0 \rho E dV \quad (3.25)$$

The rate of change of this total energy is:

$$\frac{d}{dt}\left(\int_V^0 \rho E dV\right) = \int_V^0 \frac{\partial(\rho E)}{\partial t} dV \quad (3.26)$$

The rate at which energy is convicted out of the control volume through its surface is:

$$Convective\ Flux = \int_S^0 \rho v E.ndS \quad (3.27)$$

By the Divergence Theorem, this surface integral can be converted to a volume integral:

$$\int_S^0 \rho v E.ndS = \int_V^0 \nabla.(\rho v E).dV \quad (3.28)$$

The energy balance within the control volume can be expressed as:

$$\frac{d}{dt}\left(\int_V^0 \rho E dV\right) + \int_V^0 \nabla.(\rho v E).dV = -\int_V^0 \nabla.qdV + \int_V^0 \rho v.gdV + \int_V^0 \nabla.(\mu(\nabla \mathrm{v} + (\nabla \mathrm{v})^T))dV \quad (3.29)$$

Simplifying, we get:

$$\int_V^0 \left[\frac{\partial(\rho E)}{\partial t} + \nabla.(\rho v E)\right] dV = -\int_V^0 \nabla.qdV + \int_V^0 \rho v.gdV + \int_V^0 \nabla.(\mu(\nabla \mathrm{v} + (\nabla \mathrm{v})^T))dV \quad (3.30)$$

For the equality to hold for any arbitrary control volume V, the integrands must be equal. Thus:

$$\boldsymbol{\frac{\partial(\rho E)}{\partial t} + \nabla.(\rho v E) = -\nabla.qdV + \rho v.gdV + \nabla.(\mu(\nabla \mathrm{v} + (\nabla \mathrm{v})^T} \quad (3.31)$$

Where: ρ is the density of the fluid

E is the total energy per unit mass of the fluid.

v is the velocity vector of the fluid.

q is the heat flux vector.

g is the gravitational acceleration vector.

μ is the dynamic viscosity of the fluid.

$\nabla \mathrm{v}$ is the velocity gradient tensor.

$(\nabla \mathrm{v})^T$ is the transpose of the velocity gradient tensor.

3.5 Fatigue Design approach

3.5.1 Fatigue Analysis

During the 19th-century industrial revolution in Europe, engineers began understanding metal fatigue failure. William Albert linked cyclic loads with metal strength in an article. The term "fatigue" was possibly coined by English engineer Braithwaite in 1854 or by French engineer Poncelet in 1839. Fatigue occurs after repeated load cycles, progressing through crack initiation, propagation, and failure stages. ASTM defines fatigue as progressive structural change due to fluctuating stresses, leading to cracks or fracture after many cycles. Cyclic loads cause strain, leading to elastic and plastic deformation. High stress with primarily elastic deformation results in high-cycle fatigue, while high-stress plastic deformation leads to low-cycle fatigue.

The fatigue life of a part under repeated cyclic loads is how many times it can handle stress cycles before breaking. There are three main ways to analyze fatigue life: (i) stress-life(S-N) approach for high-cycle fatigue, (ii) strain-life(e-N) approach for low-cycle fatigue, and (iii) linear elastic fracture mechanics (LEFM).

3.5.1.1 Basic terminologies of fatigue analysis

There are different cyclic load mechanism applied on the structure or solid bodies as illustrated in figure 3.11

The effect of local mean stress depends on the stress ratio, the ratio of the lowest stress to the highest stress in a fatigue load cycle. For fully reversed loading, as shown in Figure 3.11(a), the relationship between parameters is described as follows [25].

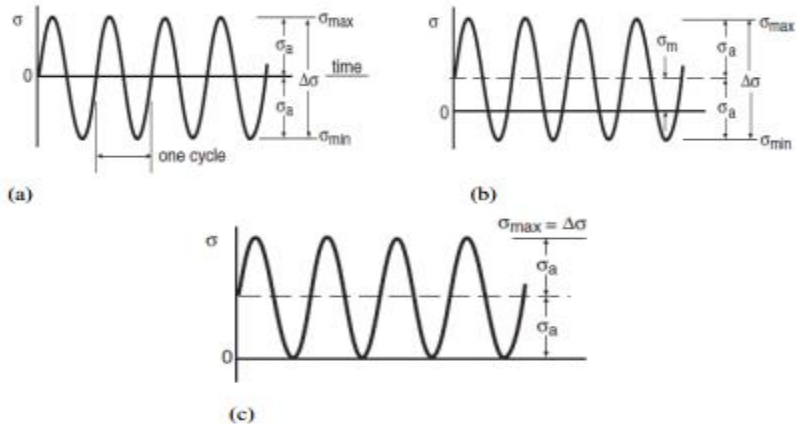

Figure 3.11 Constant amplitude cycling and the associated nomenclature [25]. Fully reversed (a), fluctuated cyclic stresses (b) and repeated (c)

$\Delta\sigma = \sigma_{max} - \sigma_{min}$ constant stress range (3.32)

$\sigma_a = \frac{\sigma_{max} + \sigma_{min}}{2}$ mean stress

$\sigma_a = \frac{\Delta\sigma}{2} = \frac{\sigma_{max} - \sigma_{min}}{2}$ stress amplitude (3.33)

$R = \frac{\sigma_{min}}{\sigma_{max}}$ stress ratio

$A = \frac{\sigma_a}{\sigma_m}$ Amplitude ratio

$\sigma_{max} = \sigma_m + \sigma_a$ Maximum stress (3.34)

$\sigma_{min} = \sigma_m - \sigma_a$ minimum stress (3.35)

Where : σ_{max} Local maximum stress in a fatigue load cycle

σ_{min} Local minimum stress in a fatigue load cycle

3.5.1.2 Stress-Life (S-N) Theory

The stress-life (S-N) analysis helps predict how long it takes for a crack to form and grow until the part breaks. The stress-life curve shows fatigue data, indicating the relationship between fatigue life (in cycles) and the stress applied. Since Kaplan hydraulic runner blades endure high cyclic loading from water flow, stress-life (S-N) analysis is used for fatigue analysis. German engineer August Wöhler developed this curve in the 1870s through systematic fatigue tests. His work laid the foundation for understanding how materials behave under repeated stress, crucial for designing durable structures like hydraulic turbine blades[26], Basquin's relation is the most widely used model, offering an analytical form of the S-N curve, especially for high-cycle fatigue[25, 29]

$$\sigma_a = \sigma'_f 2(N_f)^b \quad \text{and} \quad \sigma_a = \frac{\Delta\sigma}{2} = \frac{\Delta\varepsilon_e E}{2}$$

$$\frac{\Delta\varepsilon_e}{2} = \frac{\sigma_a}{E} = \left(\frac{\sigma'_f}{E}\right)(2N_f)^b \text{ then } N_f = \frac{1}{2}\sqrt[b]{\frac{\Delta\varepsilon_e E}{2\sigma'_f}} \quad (3.36)$$

$$b = \frac{(\log(S_e) - \log(0.9S_u))}{3} \quad (3.37)$$

Where: σ'_f Fatigue strength coefficient (for most metals it is the tensile stength),

b the fatigue exponent or Basquin exponent(-0.05 to -0.12), slope of the log-log curve

N_f number of reversals to failure

Fatigue Life (Nf) measures the number of stress cycles or strain reversals a material can endure before breaking. It typically involves three stages: (i) crack initiation near stress concentrators, (ii) gradual crack propagation, and (iii) rapid crack growth once the crack reaches a critical size. Understanding these stages is essential for designing resilient materials and structures to withstand repeated loading and avoid premature failure.

The total number of cycles to failure is the sum of cycles at the first and the second stages

$$Nf = Ni + Np \tag{3.38}$$

Where Nf represents the number of cycles to failure, Ni denotes the cycles for crack initiation and Np indicates the cycles for crack propagation. Various theories study the influence of mean stress. Basic theories include Goodman, Soderberg and Gerber. In fatigue life analysis using the S-N approach, Goodman theory is suitable for analyzing Kaplan turbine runner blades. Therefore, this study employs Goodman theory, as shown in the equation (3.39).

$$\frac{\sigma_a}{\sigma_e} + \frac{\sigma_m}{\sigma_u} = 1 \tag{3.39}$$

Where: σ_m mean stress σ_e endurance fatigue limit

σ_a stress amplitude σ_u ultimate tensile strength

3.5.2 Failure criteria

Several fatigue criteria rely on principle stresses rather than traditional engineering stress and strain. Principal stress is calculated based on the engineering stress and strain at each point. Common failure criteria include: (i) Maximum shear stress criterion (Tresca's Hexagon), (ii) Maximum Distortion Energy Criterion (Von Mises), (iii) Maximum Normal Stress Criterion (Coulomb's Criterion), and (iv) Maximum Normal Strain Criterion(St. Venant's Criteria). These criteria help to predict and prevent failures in various materials and structures [31, 32].

3.5.2.1 Von Mises Stress failure criterion:

A structure component is deemed safe if its maximum distortion energy per unit volume is lower than the distortion energy needed to induce yield in a tensile-test specimen. Von Mises stress, or Huber stress, considers all six stress components in a 3-D state of stress. Von Mises stress σ_{mv} can be calculated using six stress components, such as:

$$\sigma_{MV} = \sqrt{\frac{\left((\sigma_x-\sigma_y)^2+(\sigma_z-\sigma_x)^2+(\sigma_y-\sigma_z)^2\right)}{2} + 3\left(\tau_{xy}{}^2 + \tau_{xz}{}^2 + \tau_{yz}{}^2\right)} \quad (3.40)$$

Von Mises stress σ_{MV}, can be also expressed their principal stresses as:

$$\sigma_{MV} = \sqrt{\frac{1}{2}((\sigma_3-\sigma_1)^2 + (\sigma_1-\sigma_2)^2 + (\sigma_2-\sigma_3)^2)} \quad (3.41)$$

The maximum von Mises stress failure criterion stems from the von Mises-Hencky theory, also called the scalar-energy theory or maximum distortion energy theory. According to this theory, ductile materials begin yielding at a point when the von Mises stress equals the stress limit. Typically, the yield strength serves as this stress limit.

3.5.2.2 The Strain Energy due to Crack

As discussed earlier, the energy released from crack formation was explained using Griffith energy balance and J-integral methods.

$$J = \int_{\Gamma}^{0}\left(W dx_2 - T_i \frac{\partial U_i}{\partial X_1}\, ds\right)$$

Using the axisymmetric property at the crack tip, which matches the global coordinate system of the rotating Kaplan turbine blade (x, y), Mode I of the crack, as shown in Figure 3.12, has its J-integral expression given in equation (3.42), where ds = dxdy

$$J = \int_{\Gamma}^{0}\left(W dx_2 - \left(\sigma_{xx}\frac{\partial U}{\partial X} + \sigma_{yy}\frac{\partial V}{\partial y} + \sigma_{xy}\frac{\partial U}{\partial X}\right)\, dxdy\right) \quad (3.42)$$

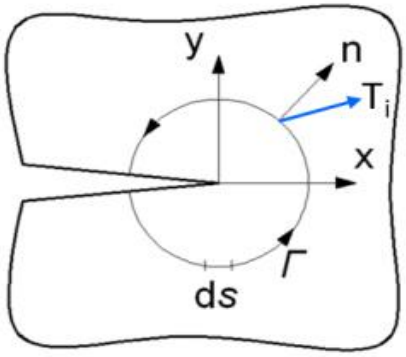

Figure 3.12 Integration path around a crack tip [43]

The loss of potential or strain energy due to crack formation on the Kaplan turbine blade can be calculated by substituting equation (3.42) into equation (3.5).

$$-\frac{d\Pi}{dA} = \int_{\Gamma}^{0}\left(Wdx_2 - \left(\sigma_{xx}\frac{\partial U}{\partial X} + \sigma_{yy}\frac{\partial V}{\partial y} + \sigma_{xy}\frac{\partial U}{\partial X}\right)\, dxdy\right) \tag{3.43}$$

Where, Π =U_C and A= A_C is area of crack

Equation (3.43) can now be simplified and reduced to the following form.

$$\frac{U_C}{dA_C} = \int_{\Gamma}^{0}\left(Wdx_2 - \left(\sigma_{xx}\frac{\partial U}{\partial X} + \sigma_{yy}\frac{\partial V}{\partial y} + \sigma_{xy}\frac{\partial U}{\partial X}\right)\, dxdy\right) \tag{3.44}$$

Equation (3.44) governs fatigue crack propagation at the fixed end of the Kaplan turbine blade. For each instance of crack growth, the energy lost is quantified by this equation. To estimate the crack's life, we can relate it to the J-Integral under plain strain conditions. Thus, equation (3.44) can be rewritten as:

$$U_C = J = -\int_{A_C}^{0}\left[\int_{\Gamma}^{0}\left(Wdx_2 - \left(\sigma_{xx}\frac{\partial U}{\partial X} + \sigma_{yy}\frac{\partial V}{\partial y} + \sigma_{xy}\frac{\partial U}{\partial X}\right)\, dxdy\right)\right] dA_C \tag{3.45}$$

The relationship between the energy release rate and the stress intensity factor (K) for Mode I fracture is given by:

$$J = \frac{1-\nu^2}{E}\Delta {K_I}^2 \tag{3.46}$$

Where, E is modulus of elasticity of the material and ν is the poisson's ratio

The relationship in equation (3.46) is used to determine the energy release rate from the stress intensity factor (K) for analytical calculations. However, in ANSYS Workbench software, if you

specify the necessary inputs for fracture analysis, you can obtain the stress intensity factor (KI) directly, along with the J value, without additional steps. Once you have the stress intensity factor (KI), you can estimate the fatigue life with increasing crack depth using Paris's law.

$$N = \int \frac{da}{C(\Delta K_I)^2} \quad (3.47)$$

Where, N is the fatigue life, da is increment in crack depth, C is constant and m is slop on the log log plot.

For a given crack depth and applied stress, the stress intensity factor is given by:

$$K_I = \sigma Y \sqrt{a} \quad (3.48)$$

Where, Y is a geometric factor which has a value of $Y = 1.12\sqrt{\pi}$ edge cracked specimen

The stress σ on the Kaplan turbine blade is the pressure exerted by the water across the blade's surface. In other words, it is the applied pressure, which can be determined from the water power input.

Material properties of Stainless steel 304 (SS 304) is given by:

$\sigma_{ulti} = 505$ Mpa $\quad K_{IC} = 283$ KJ$/m^2$

C= 1 x 10^{-12} cycle/m and m = 2.5 and the initial crack depth $a_0 = 10mm$. $K_{IC}$is the fracture toughness of the material.

Using equation 3.49, the critical crack depth can be calculated from the following equation:

$$K_{IC} = \sigma_{max} Y \sqrt{\pi a_C} \quad (3.49)$$

$$a_C = \frac{1}{\pi} \frac{{K_{IC}}^2}{Y^2 {\sigma_{max}}^2}$$

$$a_C = \frac{1}{\pi} \frac{(283)^2}{(1.12\sqrt{\pi})^2 (505)^2} = 0.0254m = 25.4mm$$

The critical crack depth of a Kaplan turbine runner blade refers to the maximum depth a crack can reach before it significantly compromises the blade's structural integrity or performance. At this

critical depth, the blade is at a high risk of failure due to the reduced ability to withstand stresses or loads.

From Paris law, the life of the runner blade can be calculated using the following sets of equations.

$$\frac{da}{dN} = C\Delta K^m = C\left(Y\Delta\sigma\sqrt{\pi a}\right)^m \quad (3.50)$$

$$\int_0^{N_f} dN = \int_{a_i}^{a_f} \frac{da}{C\left(Y\Delta\sigma\sqrt{\pi a}\right)^m}$$

Equation (3.50) can be simplified and reduced to equation (3.51). Equation (3.51) determines the lifetime of the runner blade, given an initial crack length (a_i) and a final crack length (a_f).

$$N_f = \frac{1}{C\left(Y\Delta\sigma\sqrt{\pi}\right)^m}\left[a_f - a_0\right] \quad (3.51)$$

3.6 Dynamics Fracture Mechanics

Dynamic fracture mechanics studies fractures in which material inertia and time-based behavior are critical. This consists of cases with rapid loading on cracks or quick crack propagation near the crack tip. These situations emphasize inertial effects because of rapid loading or crack motion [30, 18].

Dynamic fracture takes place whilst material behavior turns into time-structured, loads are implemented rapidly, or cracks propagate rapidly. When a majority of these elements coincide, the evaluation becomes substantially extra complex. Rapid loading transmits strain waves to the crack, magnifying its influence on the fracture process. Understanding these interactions is important for accurately predicting and managing fractures in materials below dynamic conditions, wherein the speed of crack propagation and the reaction to unexpected loading play vital roles inside the structural integrity and failure mechanisms of the material [30]. Stress waves propagate through substances and replicate off surfaces like obstacles and crack planes. These reflections alter nearby stress and pressure near the crack tip, immediately impacting fracture behavior [18, 30].

Dynamic fracture takes place while substances behave otherwise over time, loads are carried out fast, and cracks expansion. Studying these situations wishes advanced evaluation because these elements interact in complicated ways. When hundreds are implemented swiftly, pressure waves carry the weight to the crack. These waves circulate through the material, bouncing off edges and

crack surfaces. When they get better, they exchange the stress and strain near the crack's tip, affecting how the material breaks [33, 34].

To predict crack development beneath strain wave loading, one should calculate the brief driving force on the crack faces. During fast crack propagation, particles on opposite crack faces displace relative to each other after the crack part passes [30].

Mott first proposed dynamic fracture, considering the kinetic energy of crack increase causing inertial consequences in deformable bodies. He analyzed this the usage of pressure waves within elastic cracked bodies [30, 35, 36].

3.6.1 Causes of Dynamic loading

The dynamic loading of Kaplan turbine runner blades in most cases originates from numerous resources related to the operation and design of the turbine. According to Vigants those supply consists of:

Firstly, the rotational pace of the turbine rotor creates centrifugal forces that act at the blades. These forces range with the velocity of the turbine and can result in dynamic stresses at the blades.

Secondly, hydraulic forces because of water glide through the turbine blades make a contribution significantly to dynamic loading. The high-strain water flow exerts forces at the blades as it passes through, causing various stresses depending at the flow charge and stress situations.

Additionally, the interaction among the water flow and the blades can lead to cavitation results. Cavitation occurs when the local pressure drops underneath the vapor strain of water, causing the formation and fall apart of vapor bubbles near the blade surfaces. These collapses produce severe localized stress pulses, ensuing in dynamic loads at the blades.

Furthermore, operational situations such as start-up, shutdown, and load adjustments can introduce brief loads on the blades, affecting their dynamic behavior.

3.6.2 Elastic-plastic dynamics

Elastic-plastic dynamics in Kaplan hydraulic turbine runner blades discuss with the mechanical behavior of those components below variable flow conditions, wherein the material undergoes both elastic and plastic deformations. In elastic-plastic analysis, the material to begin with deforms elastically until reaching its yield factor, beyond which plastic deformation takes place.

Elastic-plastic dynamics of Kaplan hydraulic turbine runner blades discuss with the look at of ways these blades respond to mechanical loads, experiencing both reversible (elastic) and irreversible (plastic) deformations under various flow rates and operating conditions.

3.7 Design of the runner blade

3.7.1 Design specification for Porjus U9 turbine

Developing complex-shaped three-dimensional blades is crucial for advancing the analysis of fatigue growth rate and estimating fracture lifetime using ANSYS. Utilizing the NACA 4412 airfoil profile, a 3D solid model of the runner blade is created. NACA 4412, a symmetric airfoil profile, is extensively employed in aerodynamic and hydrodynamic applications. Its design offers a harmonious blend of lift, drag, and stall properties, rendering it widely favored in engineering for its efficient and predictable aerodynamic performance. By employing this profile to construct the runner blade model, engineers can accurately simulate and analyze fatigue characteristics, contributing to the optimization and durability of various mechanical systems, such as turbines and propellers.

Taking the loading conditions data from Porjus U9 turbine [38] all the other design specifications are evaluated from the given main specification of the turbine.

Table 3.1 Kaplan turbine runner blade technical specification for Porjus U9 turbine [38]

Technical specification	**Value**
Diameter of Runner	1.55m
Number of blade	6
Power output at high load	10MW
Operational Head	55m
Net Head	7.5m
Flow rate	$20m^3/sec$
Turbine speed	600 rpm
Overall efficiency	0.93

Calculated suction head will be (H_S) = 0.673

Head = Net head + Suction head

Head = 7.5m + 0.673m = 8.173m

The Profile geometrical data was developed in the form of coordinate points in x-axis, y-axis and z-axis.

Blade design relies heavily on stress analysis and various other factors. The leading edge is thicker than the trailing edge to ensure streamlined flow. Maintaining thinness enhances cavitation characteristics, with thickness increasing from the hub to the tip. Additionally, blades are twisted to align with tangential velocity. These considerations ensure optimal performance and durability in various applications, like turbines and propellers, by minimizing stress concentrations, maximizing fluid dynamics efficiency, and mitigating issues like cavitation.

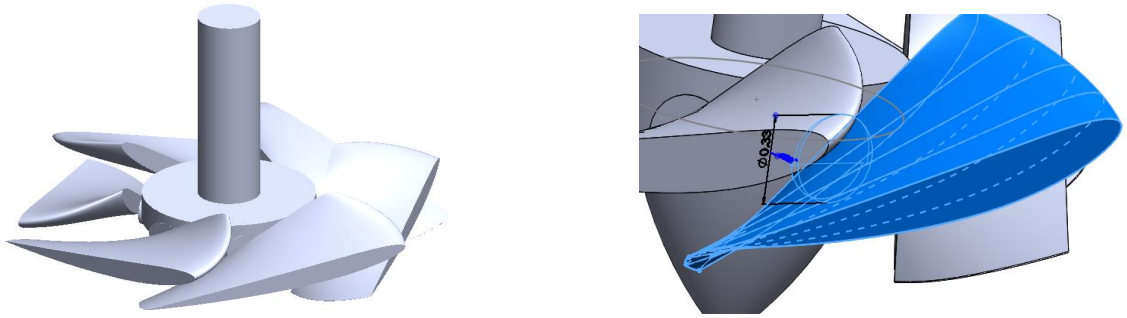

a. plane view of runner blade b. plane view of turbine runner

Figure 3.13 Kaplan turbine runner blade

3.7.2 Twist of the Blade under Ideal Circumstances

Velocity triangles on the runner blade, decomposing fluid flow velocities into components, are crucial for determining blade twist. With axial flow velocity at inlet and outlet (w1=w2=w), these triangles guide the design, ensuring optimal blade alignment for efficient energy conversion in turbines and propulsion systems.

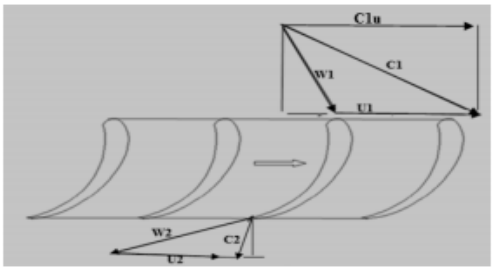

Figure 3.14 Velocity triangle at entry and exit of an axial flow Kaplan turbine runner blade

When a cylindrical cut is made at the runner, it forms a grating-like pattern as shown in Figure 3.15. Velocity triangle 1 is just before the grating, and velocity triangle 2 is just after. The meridian components, w1m and w2m, are equal. The medial relative velocity, determined by averaging w1 and w2, is directed according to angle β∞. The parameter t indicates the grating partition, while l represents the chord length. These factors help understand and optimize fluid flow characteristics, aiding in the design and performance enhancement of turbines and similar systems.

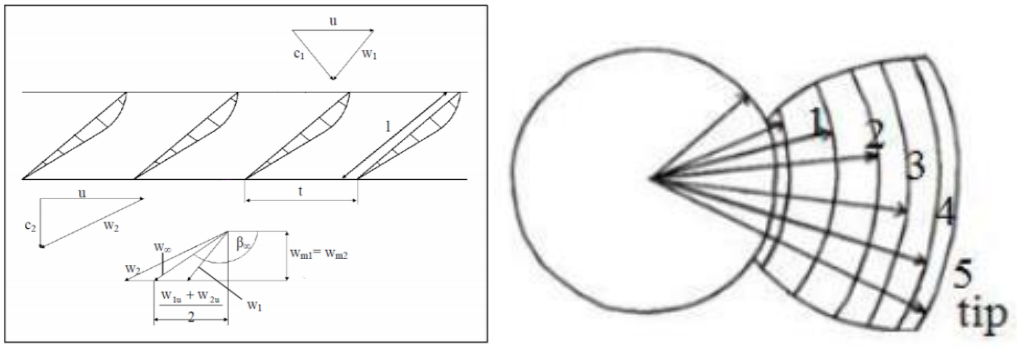

a. Grating(velocity triangle) b. Five sections of the blade

Figure 3.15 Velocity triangle and blade section [3, 37,28]

Defining the runner blade's twist involves determining five blade diameters using velocity triangles, followed by establishing the angle β∞ and chord length for each radius. Lofting is then performed to draw conclusions on the blade's twist. Table3.4 displays velocities and significant angles of the velocity triangles for each diameter [39].

$r_1 = \frac{d}{2} + 0.015D$ Section 1 (3.52)

$r_3 = \frac{d}{2}\sqrt{\frac{1+\left(\frac{d}{2}\right)^2}{2}}$ Section 3 (3.53)

$r_2 = r_1 + \frac{r3-r1}{2}$ Section 2 (3.54)

$r_5 = \frac{D}{2} - 0.015D$ Section 5 (3.55)

$r_4 = r_3 + \frac{r5-r3}{2}$ Section 4 (3.56)

$U=\pi \times n \times D$ $Wm=\frac{Q}{A}$ $\beta\infty = 90 - tan^{-1}\left(\frac{Wu\infty}{Wm}\right)$

$Cu=H\infty \times \frac{g}{U}$ $W=\sqrt{Wu^2 + Wm^2}$ $t = \frac{\pi D}{z}$ $l = 0.75\ t$

$Wu= Cu-u$ $Wu\infty = \frac{Wu1+Wu2}{2}$ and $W\infty = \sqrt{Wu\infty^2 + Wm^2}$

Where:

r radius of the partial blade [m]

U The tangential velocity of the blade [m/s]

Cu The tangential velocity of the fluid flow [m/s]

Wu The tangential relative velocities [m/s]

Wm The relative velocity in meridian direction [m/s]

W The relative velocity at the middle of the blade [m/s]

Wu∞ The relative velocity in the tangential direction [m/s]

$\beta\infty$ The angle at the middle of the blade with horizontal [^{o}]

l chord length [m]

t blade spacing [m]

D runner diameter

[m]

Table 3.2 Details of the theoretical runner design (See Appendix A)

Symbol	D_{hub}	1	2	3	4	5	D_{tip}
D(m)	0.775	0.8216	1.0236	1.2254	1.3644	1.5036	1.55
U(m/sec)	24.35	25.81	32.16	38.50	42.86	47.24	48.69
Cu1(m/sec)	2.99	2.82	2.27	1.89	1.70	1.54	1.5
Cu2(m/sec)	3.05	2.88	2.31	1.93	1.73	1.57	1.53

Wu1(m/sec)	-21.36	-22.99	-29.89	-36.61	-41.16	-45.7	-47.19
Wu2(m/sec)	-21.3	-22.93	-29.85	-36.57	-41.13	-45.67	-47.16
Cu∞(m/sec)	3.02	2.85	2.29	1.91	1.72	1.56	1.51
Wu∞(m/sec)	-21.33	-22.96	-29.87	-36.59	-41.145	-45.685	-47.175
Wm(m/sec)	14.15	14.15	14.15	14.15	14.15	14.15	14.15
W1(m/sec)	25.62	26.99	33.07	39.25	43.52	47.84	49.27
W2(m/sec)	25.57	26.95	33.03	39.21	43.496	47.81	49.24
W∞(m/sec)	25.597	26.97	33.05	39.23	43.51	47.83	49.25
$\beta\infty$(degree)	146	148	155	159	161	162	163
$\beta 1$	146.5	148.4	154.7	158.9	161	162.8	163.3
$\beta 2$	146.4	148.3	154.6	158.9	161	162.78	163.3
(180−$\beta\infty$)deg.	34	32	25	21	19	18	17
t	0.406	0.43	0.536	0.642	0.714	0.787	0.812
l	0.3045	0.3225	0.402	0.4815	0.5355	0.5903	0.609

3.7.3 Force calculation

The various types of forces are applied on the hydraulic kaplan turbine runner blade as calculated below

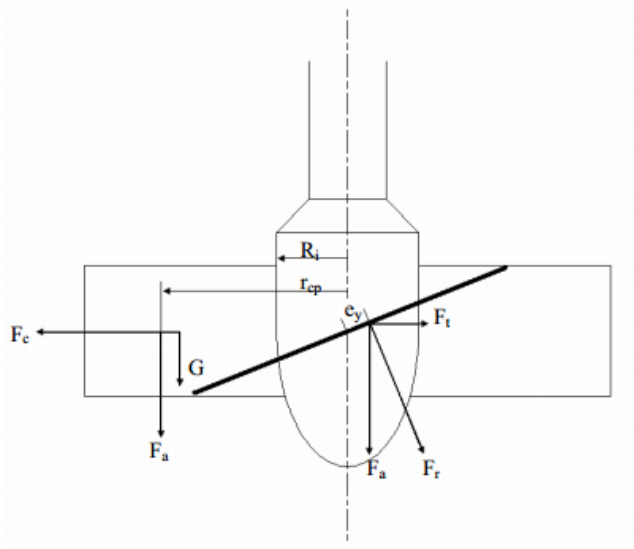

Figure 3.16 Occurring forces upon the blade[37, 28]

radius of the center of pressure

The radius $\mathbf{r_{cp}}$ can be calculated using the following equation:

$$r_{cp} = \sqrt{\frac{Dr^2 + Dh^2}{2}} \quad \text{[m]} \quad (3.57)$$

Where

Dr	runner diameter	[m]
Dh	hub diameter	[m]

A resulting radius of the center of pressure **1.23m** results from the equation (3.57)

Centrifugal force

An inertial force which tends to pull an object outward when it is in orbit or is rotating around a center is centrifugal force

$$Fc = mrw^2 \quad \text{[N]} \quad (3.58)$$

Where

m	mass of the blade	[Kg]
r	radius of the runner	[m]
w	Angular velocity	[rad/s]

Take m= 525kg and ε=20^o from litrature [42]

A resulting centrifugal force from equation (3.58) is $\mathbf{9.3 * 10^4\ N}$

Water force

Water force that applied on the runner blade is calculated below

$$Fw = \rho Qrw \quad \text{[N]} \quad (3.59)$$

Where

ρ	Density of water	[kg/m^3]

Q Flow rate [m^3/s]

r radius of the runner [m]

w Angular velocity [rad/s]

A resulting water force of $\mathbf{3.58 * 10^6 N}$ results from the equation (3.59)

Tangential component of water force

$Fwt = Fw \cos\varepsilon$ [N] (3.60)

Where

Fw water force [N]

A resulting tangential component of water force of $\mathbf{3.36 * 10^6 N}$ results from the equation (3.60)

Axial component of water force

$Fwa = Fw \sin\varepsilon$ [N] (3.61)

Where

Fw water force [N]

A resulting Axial component of water force of $\mathbf{1.22 * 10^6 N}$ results from the equation (3.61)

Pressure

Pessure applied on the runner blade is calculated below

$P = \frac{Fw}{A}$ [Pa] (3.62)

Where

Fw water force [N]

A Area [m^2]

A resulting pressure of $\mathbf{2.53 Mpa}$ results from the equation (3.62)

Resulting force

The force $\boldsymbol{Fr}$ can be established by using the following equation:

$$Fr = \sqrt{Fwt^2 + Fwa^2} \quad [N] \quad (3.63)$$

A resulting force of $\mathbf{3.58 * 10^6}$N results from the equation (3.63)

The force Fr causes a turning moment which tends to turn the blade about its axis of rotation - the 'hydraulic moment'. The value of the moment changes due to the adjustment of the blade. The main forces that the adaptation mechanism has to withstand are caused by this moment. Hence, the moment has a high influence on the design of the adaptation mechanism and can be calculated with the following equation:

$$M_h = Fr * e_y \quad [Nm] \quad [3.64]$$

Where

e_y distance from the Cp to the rotation axis of the blade [m]

The center of pressure cp is not a fixed point; it changes its position depending on the adjustment of the blade. Thus the arm e_y also changes its value. Under simplified circumstances as those in equation 3.65, the arm e_y can be calculated, although the evaluation is not 100% accurate. The exactly center of pressure and consequently the exactly length of the arm e_y can only be precisely established by using model tests. However, to get an idea of the length of e_y the calculation under simplified circumstances is sufficient.

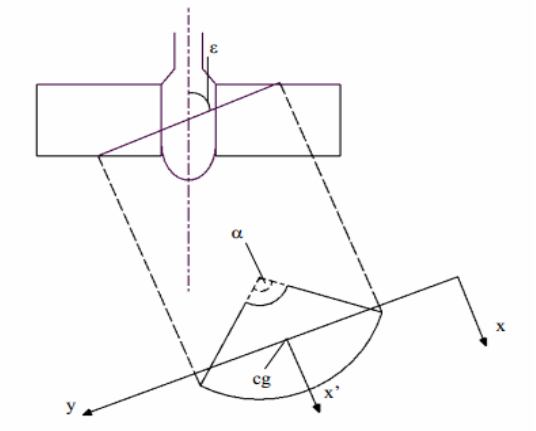

Figure 3.17 Turbine with projected view of the blade[3,37, 28]

The distance between the center of gravity cg and respectively the rotation axis of the blade and the center of pressure in y-direction can be calculated with the following equation:

$$e_y = \frac{I_s}{y_s * Ab} \quad [m] \quad [3.65]$$

Where

I_s moment of inertia of the area A related to the x'-axis which runs parallel to the x-axis over the center of gravity [m^4]

y_s the distance between the x-axis and the center of gravity [m]

A_b area of the blade [m^2]

The moment of inertia is defined as:

$$I_s = \frac{{R_r}^4 - {R_h}^4}{4} \times \left(\frac{\hat{\alpha}}{2} - sin\frac{\alpha}{2} \times cos\frac{\alpha}{2}\right) \quad [m^4] \quad (3.66)$$

With a blade-radius R_r of 1.55 m, hub-radius R_h of 0.775 and an angle α of 80°($\hat{\alpha} = 1.396$) a moment of inertia of $\mathbf{0.2776}\boldsymbol{m^4}$ results.

The distance y_s can be calculated as follows:

$$y_s = \frac{F_a}{g \times \rho \times A_b \times cos\varepsilon} \quad [m] \quad [3.67]$$

Where

F_a force of the water on the plate [N]

g acceleration of gravity [m/s^2]

ρ water density [kg/m^3]

A_b area of the blade [m^2]

ε angle of the adjustment of the blade [°]

Angle ε changes with the adjustment of the blade. The smaller the angle the bigger is e_y. The smallest possible angle of 20° was chosen. Hence, a y_s of $\mathbf{2.75} * \mathbf{10^2}\ \boldsymbol{m}$ results.

All the necessary values are now known to calculate e_y - a value of $\mathbf{0.0019}\ \boldsymbol{m}$ results from the equation (3.65)

Using the results from equation (3.65) and (3.66) in equation (3.67) a maximum turning moment (See Appendix A) of $\mathbf{6.53} * \mathbf{10^3 Nm}$ results.

Chapter Four

4. Numerical Analysis

4.1 Numerical Analysis Using ANSYS

ANSYS is a versatile FEA software program used for fixing complicated engineering issues. Developed from the technique delivered by using Turner et al. In 1956, FEA is a computational method that approximates answers for structures with complicated geometries and numerous boundary situations [40].

Finite Element Analysis (FEA) is a numerical approach that breaks down a complex device into smaller, manageable devices known as elements. The software program applies and solves the governing equations for every element, integrating those answers to offer a detailed understanding of the system's overall behavior. Results may be displayed in tables or graphs. This approach is in particular beneficial for designing and optimizing structures too complicated for manual analysis due to their difficult geometry, scale, or governing equations. FEA software presents a comprehensive set of gear for modeling detail behavior, material properties, and solving equations throughout numerous engineering challenges.

Basic Steps used in the solution procedure using ANSYS are the following:

Building Geometry: The geometry of the hydro Kaplan turbine runner blade is imported in STEP AP203 (Standard for the exchange of product model data, Application protocol 203) format for analysis. STEP AP203 is a standard document layout used to transfer 3D geometric statistics among one of a kind CAD and analysis software program. By uploading the runner blade's geometry on this layout, the right form, dimensions, and details of the blade are correctly added into the analysis surroundings.

Defining of Material Properties: The material properties of the runner blade are specified to define how the blade will respond to numerous forces and situations throughout operation. This consists of key attributes like Young's modulus (which measures stiffness), Poisson's ratio (which describes the material's deformation in perpendicular directions), and density (which impacts the blade's weight). By specifying those properties, the analysis software program can accurately simulate the blade's behavior underneath stress, pressure, and different operational factors.

Generating Mesh: Meshing of the three-dimensional (3D) Kaplan turbine runner blade model includes dividing the complex geometric shape into smaller, viable elements or cells. This procedure transforms the continuous geometry right into a finite detail mesh, that's essential for numerical evaluation. Each element inside the mesh represents a portion of the blade and allow the simulation software program to approximate how forces and conditions affect the blade. The quality and density of the mesh effect the accuracy of the evaluation.

Boundary circumstance and Applying Loads: Boundary situations and outside loads are implemented to define how the Kaplan turbine runner blade interacts with its environment all through simulation. Boundary situations specify constraints which includes fixed supports or rotational constraints, representing how the blade is installed or related. External loads include forces, pressures, and other operational influences that act at the blade, including water flow forces or centrifugal forces.

Reading the Solution: The solution is generated primarily based at the preceding input parameters by means of walking the simulation using the described geometry, material properties, boundary situations, and external loads. This process involves the numerical solving of equations that represent how the Kaplan turbine runner blade will behave underneath distinctive situations.

4.1.1 Geometrical Modeling of the Kaplan turbine runner blade

Given the complicated shape of the Kaplan turbine blade, MATLAB 2014 was employed to deal with the complexity. By going for runs specific MATLAB code, a text report become generated, which incorporates particular coordinates of the blade profile at various chord lengths and angles. This facts was essential for developing an accurate 3-D model. Concurrently, SolidWorks 2021 turned into used to model the 3-dimensional geometry of the runner blade. The ensuing version, depicted in Figure 4.1b, illustrates the Kaplan turbine runner blade with none cracks. In this version, the blade is shown assembled with the runner, supplying a comprehensive view of the entire thing.

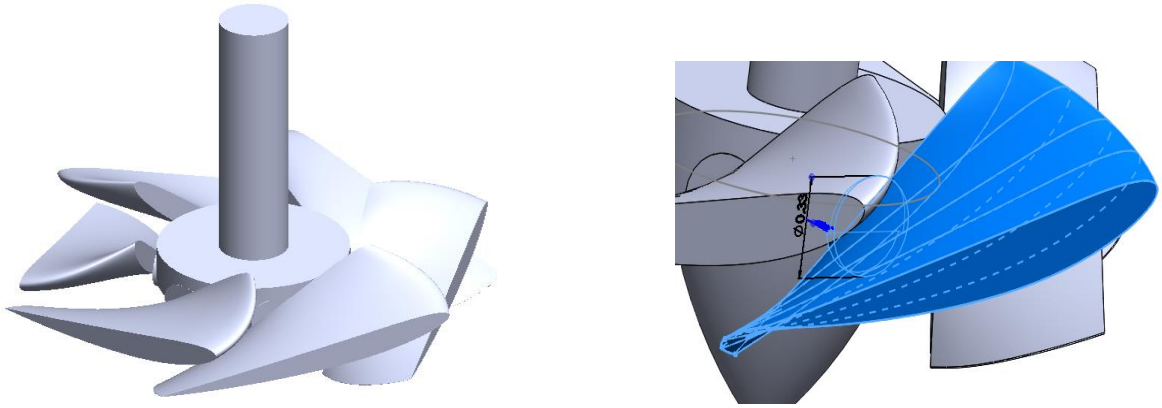

Figure 4.1a Kaplan turbine

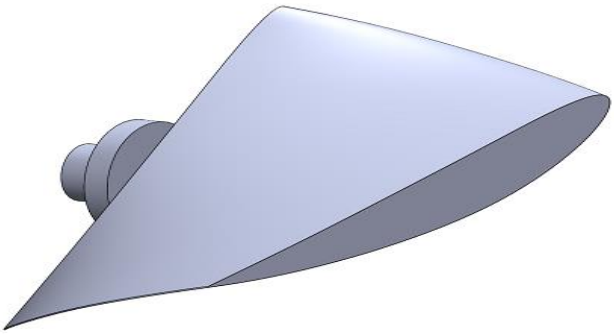

Figure 4.1b Kaplan turbine runner blade

Figure 4.1 Kapalan turbine and runner blade

4.1.2 Defining of Material Properties

The Kaplan turbine runner blade is made from stainless steel 304 (SS 304). The necessary material properties for the analysis are provided in Table 4.1

Table 4.1 material properties of stainless steel 304

$\rho(^{kg}/_{m^3})$	E(Gpa)	$\mu(Gpa)$	$\sigma_{ulti-tens}(Mpa)$	$\sigma_{tens\_yild}(Mpa)$	$K_{Ic}(^{KJ}/_{m^2})$	v
8000	193	77	505	215	283	0.33

4.1.3 Generating Mesh

The default mesh settings had been determined inadequate for reaching correct outcomes within the analysis. To ensure precision, a refined meshing approach was followed. Specifically, nice meshing was carried out to the place around the crack tip, whilst a global mesh was used for the ultimate structure. For the crack area, the "Sizing" alternative within the menu turned into utilized

to obtain a high-resolution mesh. The detail length for areas outside the crack surfaces was set to 2 mm. In contrast, a sphere of have an impact on type become hired near the elliptical crack surface, with a radius of 1 mm and an element size of 0.8 mm. Additionally, a patch conforming set of rules turned into used to similarly enhance mesh quality.

According to ANSYS 2021R1 suggestions for fracture problems, tetrahedral elements were used for the regions far from the crack, whereas hexahedral mesh became carried out specifically to the fracture module. This technique guarantees that the mesh is adequately distinct to capture the complex strain distributions and crack behavior appropriately.

The quantity of meshing affects each the accuracy and period of the evaluation. A finer mesh provides more correct results however appreciably increases analysis time.

Table 4.2(a) indicates that the whole body was meshed the usage of the tetrahedral method. Table 4.2(b) gives details at the body sizing, specifying the detail (element) sizes used. Having created a local coordinate system for crack location, a sphere of influence is used and a fined is used for regions near to the crack as it can be shown in Table(c) For the crack evaluation, a local coordinate system turned into created to accurately function the crack. Figure 4.2 illustrates the mesh for the runner blade without a crack, whilst Figure 4.3 presentations the mesh in particular around the crack. This method ensures a detailed and accurate analysis through focusing on the critical regions in which the crack is located.

Table 4.2 details of mesh in ANSYS workbench

(a)

Details of "Patch Conforming Method" - Method	
Scope	
Scoping Method	Geometry Selection
Geometry	1 Body
Definition	
Suppressed	No
Method	Tetrahedrons
Algorithm	Patch Conforming
Element Order	Quadratic

(b)

Details of "Mesh"	
Display	
Display Style	Use Geometry Setting
Defaults	
Physics Preference	Mechanical
Element Order	Program Controlled
Element Size	0.8 mm
Sizing	
Quality	
Inflation	
Advanced	

(c)

Details of "Body Sizing" - Sizing	
Scope	
Scoping Method	Geometry Selection
Geometry	1 Body
Definition	
Suppressed	No
Type	Sphere of Influence
Sphere Center	Coordinate System
Sphere Radius	2.0 mm
Element Size	0.7 mm

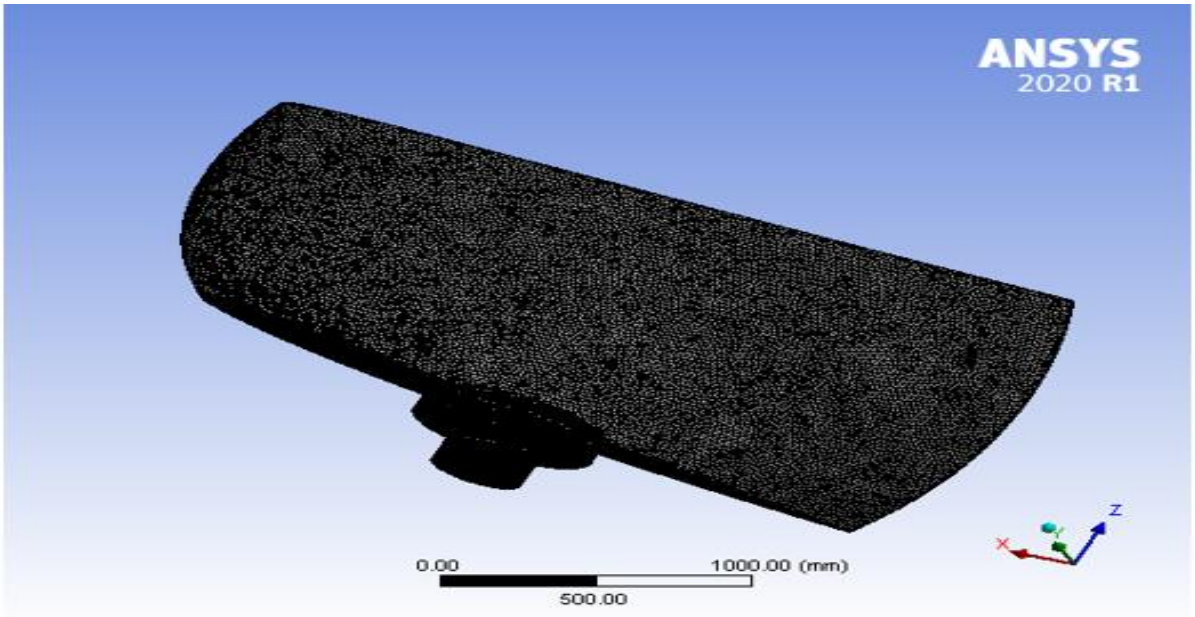

Figure 4.2 Meshed runner blade without crack

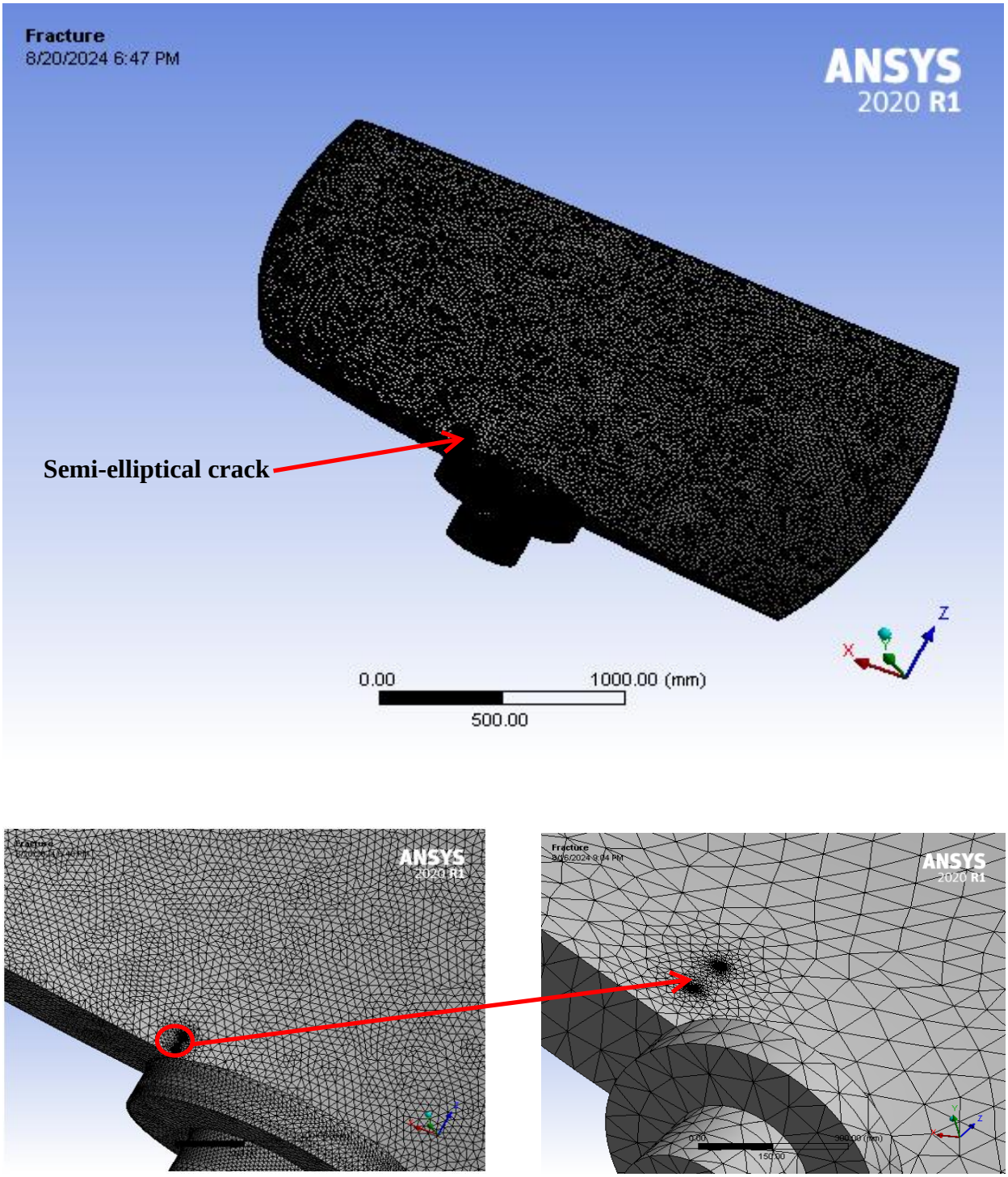

Figure 4.3 Meshed runner blade with crack

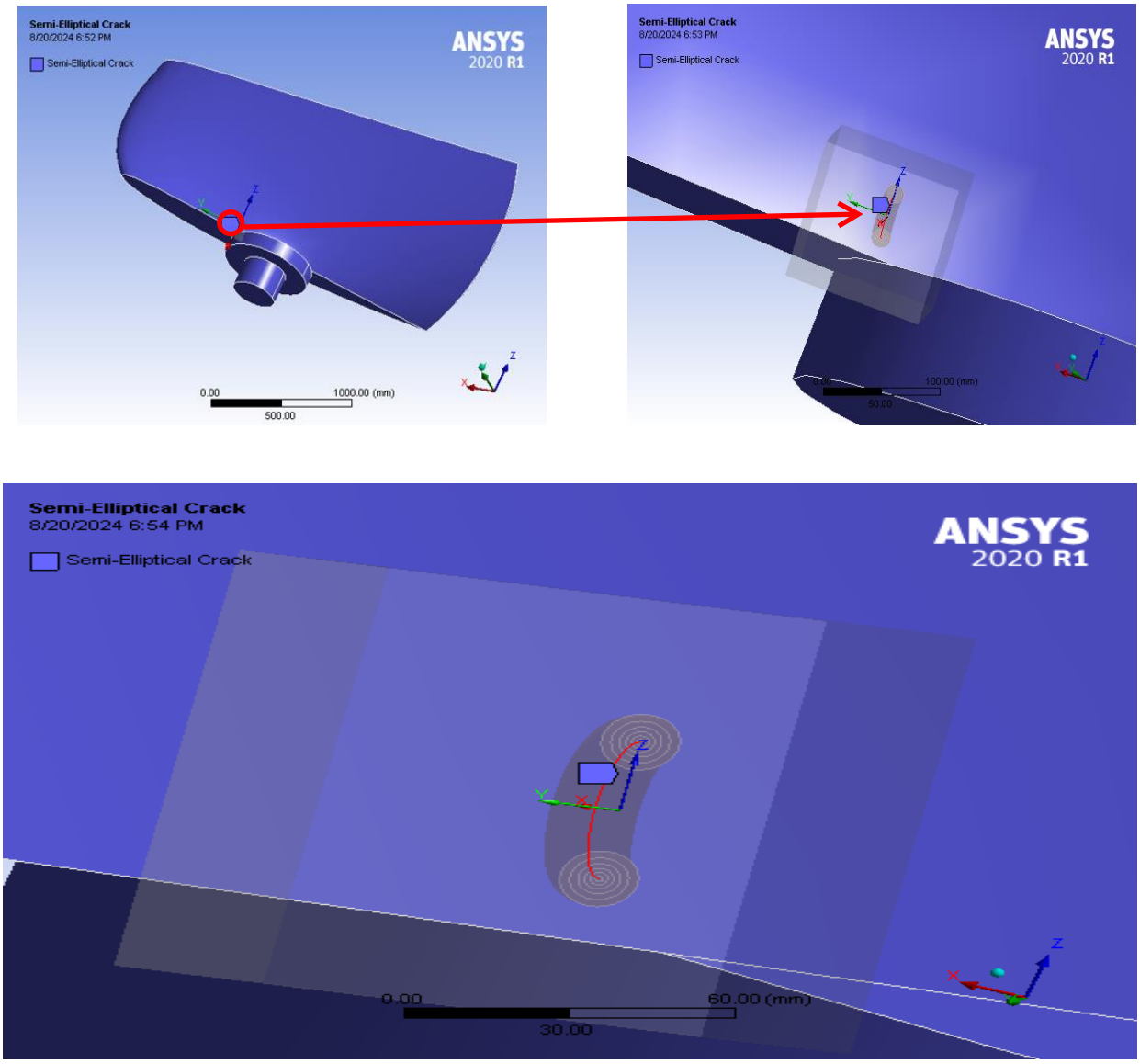

Figure 4.4 Meshed runner blade around a crack region

4.1.4 Boundary condition and Applying Loads

As previously discussed, the Kaplan runner blade is modeled as a cantilever beam with one end fixed and the other end free. During operation, a water load exerts a pressure of 2.53 MPa on the surface of the runner blade. Additionally, the angular velocity of the runner blade is set at 231.4 rad/s, with rotation occurring around the Y-axis. This rotational force is applied continuously during each revolution, as shown in Figure 4.5

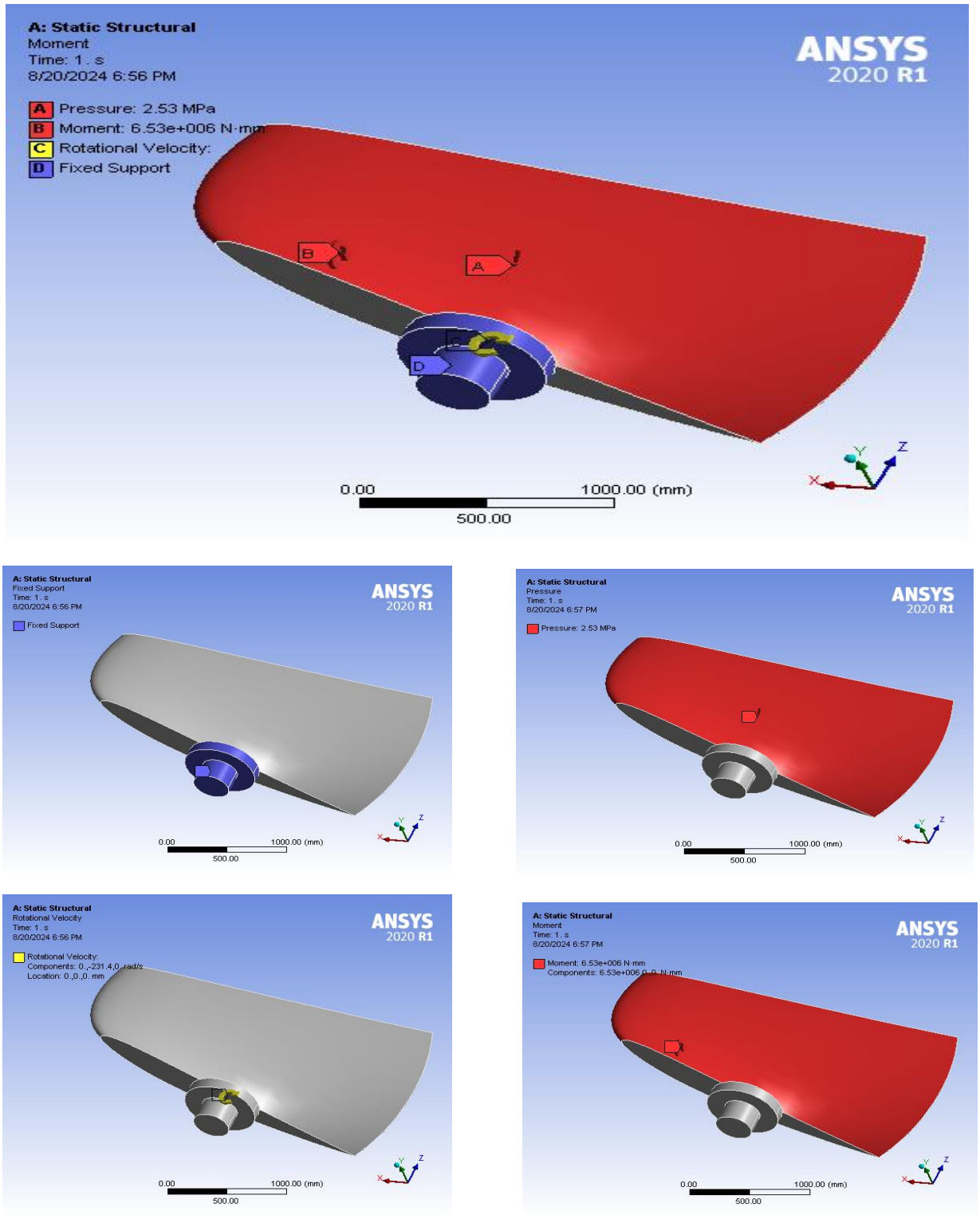

Figure 4.5 Boundary and loading conditions of Kaplan turbine runner blade

Chapter Five

5. Result and Discussion

5.1 Investigation of Fatigue growth rate

Taking near the root area of the runner blade surface as a point of interest, a semi- elliptical crack was assumed to be initiated near the root area on the surface of the blade. The initiated crack length (Major radius b) was taken to be 2 mm and crack depth (minor radius a) of 1mm.

Dimensions of the crack are calculated using the crack aspect ratio a/b. As shown in table 5.1, the crack aspect ratio and crack depth are related based on crack length. After b= 48.58, since it's the maximum crack length, the crack depth will increase 1 mm.

Table 5.1 Crack model summary

crack length(mm)	Crack Aspect Ratio(a/b)	Crack depth(mm)
0	0.5	0
0.79623	0.5	0.398115
1	0.5	0.5
2	0.5	1
3	0.5	1.5
4	0.5	2
5	0.5	2.5
6	0.5	3
7	0.5	3.5
8	0.5	4
9	0.5	4.5
10	0.5	5
11	0.5	5.5
12	0.5	6
13	0.5	6.5
14	0.5	7
15	0.5	7.5
16	0.5	8
17	0.5	8.5
18	0.5	9
19	0.5	9.5
20	0.5	10
21	0.5	10.5
22	0.5	11

23	0.5	11.5
24	0.5	12
25	0.5	12.5
26	0.5	13
27	0.5	13.5
28	0.5	14
29	0.5	14.5
30	0.5	15
31	0.5	15.5
32	0.5	16
33	0.5	16.5
34	0.5	17
35	0.5	17.5
36	0.5	18
37	0.5	18.5
38	0.5	19
39	0.5	19.5
40	0.5	20
41	0.5	20.5
42	0.5	21
43	0.5	21.5
44	0.5	22
45	0.5	22.5
46	0.5	23
47.386	0.5	23.693
47.784	0.5	23.892
48.182	0.5	24.091
48.58	0.5	24.29

The most von Mises stress in a Kaplan turbine runner blade is normally found at locations wherein stress concentrations occur due to geometric functions and loading conditions. One common area in which most stress is observed is at the basis of the runner blade.

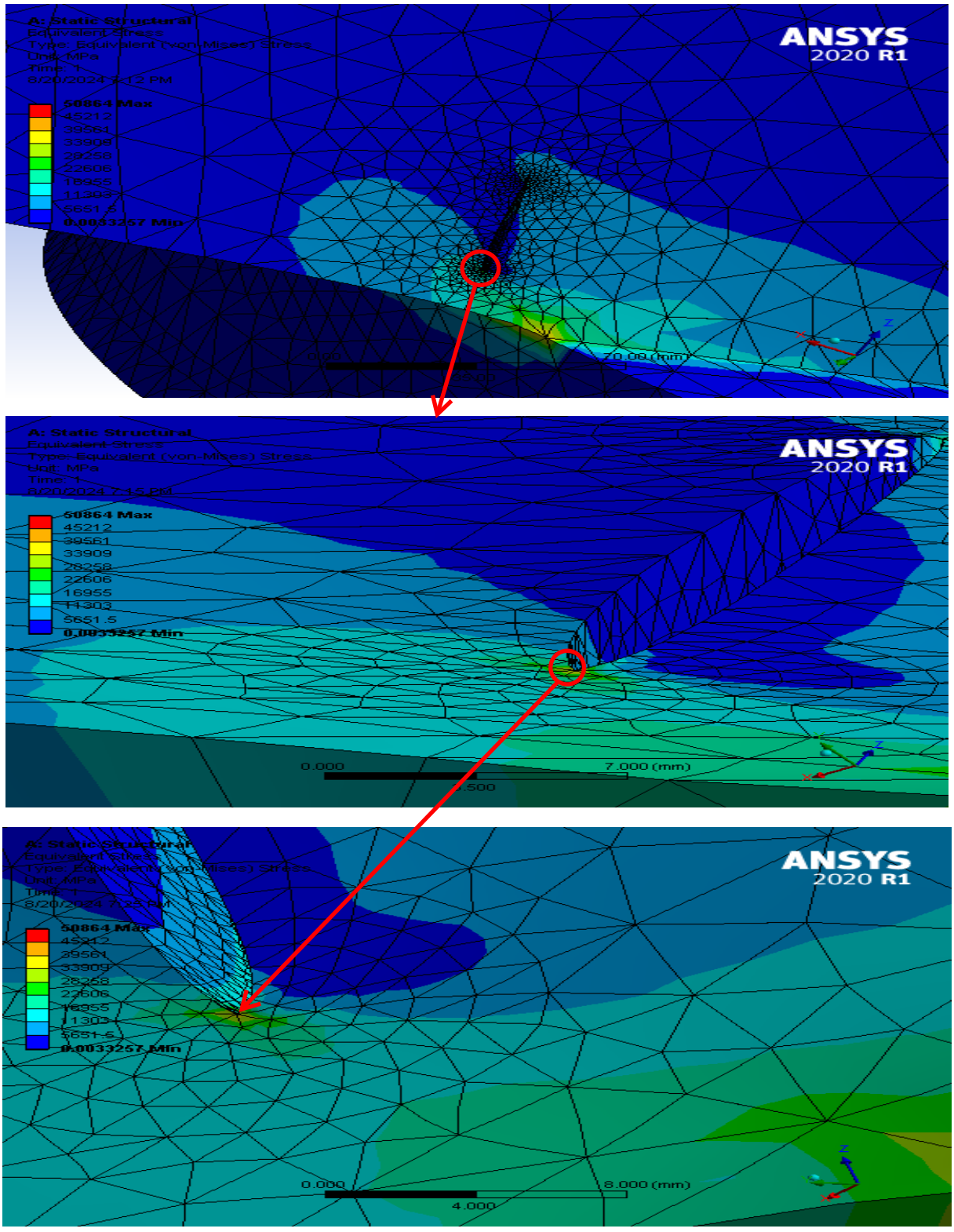

Figure 5.1 Von-mises stress distribution on the runner blade

5.1.1 Fatigue Growth rate Analysis

From the above figure 5.1 for each increment of crack depth, exclusive fracture parameters are calculated and depicted in Table 5.2. Even though the critical crack intensity is 25.4mm, the Ansys workbench fracture module couldn't study the value of crack intensity above 24.29 mm. Therefore, the analysis is accomplished until 24.29 mm of crack depth. However, the fracture of the runner blade is inevitable to occur while the crack depth reaches 25.4mm.

$$\frac{da}{dN} = C(\Delta K_I)^m \quad (5.1)$$

$$dN = \int_{a_o}^{a_f} \frac{da}{C(\Delta K_I)^m} \quad (5.2)$$

$$N_i = N_j + dN_i \qquad \text{where i = 1,2,3,… j = 0,1,2,3….} \quad (5.3)$$

Table 5.2 Different fracture parameters vs crack depth

crack depth(mm)	Crack step	C	m	ΔK_I(MPa√mm)	da/dN (mm/cycle)	dN (cycle)	N (cycle)
0	0	1E-15	2.5	1768	1.31433E-07	0	0
0.398115	1	1E-15	2.5	1847	1.46611E-07	5430893.6	5430893.647
0.5	2	1E-15	2.5	1930	1.63641E-07	1245222.5	6676116.186
1	3	1E-15	2.5	2031	1.85898E-07	5379292.9	12055409.08
1.5	4	1E-15	2.5	1965	1.71162E-07	5842431.3	17897840.36
2	5	1E-15	2.5	2078	1.9684E-07	5080262.4	22978102.73
2.5	6	1E-15	2.5	2160	2.16837E-07	4611748.6	27589851.31
3	7	1E-15	2.5	2109	2.04264E-07	4895629.6	32485480.89
3.5	8	1E-15	2.5	2100	2.02092E-07	4948251.5	37433732.37
4	9	1E-15	2.5	2279	2.47948E-07	4033101.8	41466834.2
4.5	10	1E-15	2.5	2383	2.77211E-07	3607363.4	45074197.59
5	11	1E-15	2.5	2442	2.94689E-07	3393406.2	48467603.81
5.5	12	1E-15	2.5	2438	2.93484E-07	3407342.2	51874945.97
6	13	1E-15	2.5	2546	3.27074E-07	3057412.3	54932358.22
6.5	14	1E-15	2.5	2598	3.44031E-07	2906712.9	57839071.09
7	15	1E-15	2.5	2593	3.42378E-07	2920745.4	60759816.53
7.5	16	1E-15	2.5	2717	3.8479E-07	2598818.2	63358634.76
8	17	1E-15	2.5	2783	4.08586E-07	2447467.8	65806102.55
8.5	18	1E-15	2.5	2761	4.00559E-07	2496513.9	68302616.42
9	19	1E-15	2.5	2920	4.60741E-07	2170415.4	70473031.86

9.5	20	1E-15	2.5	2939	4.68273E-07	2135507.2	72608539.04
10	21	1E-15	2.5	2953	4.73869E-07	2110286.3	74718825.35
10.5	22	1E-15	2.5	3057	5.167E-07	1935358.4	76654183.76
11	23	1E-15	2.5	3091	5.31187E-07	1882575.9	78536759.63
11.5	24	1E-15	2.5	3094	5.32477E-07	1878015.7	80414775.36
12	25	1E-15	2.5	3123	5.45042E-07	1834721	82249496.39
12.5	26	1E-15	2.5	3134	5.49854E-07	1818664.2	84068160.6
13	27	1E-15	2.5	3179	5.69805E-07	1754986.1	85823146.7
13.5	28	1E-15	2.5	3301	6.26057E-07	1597298.9	87420445.58
14	29	1E-15	2.5	3595	7.74903E-07	1290484.4	88710930
14.5	30	1E-15	2.5	3580	7.66845E-07	1304044.6	90014974.56
15	31	1E-15	2.5	3451	6.9962E-07	1429346.8	91444321.32
15.5	32	1E-15	2.5	3544	7.47712E-07	1337413.5	92781734.87
16	33	1E-15	2.5	3647	8.03229E-07	1244974.9	94026709.75
16.5	34	1E-15	2.5	3706	8.3611E-07	1196014.5	95222724.3
17	35	1E-15	2.5	3776	8.76153E-07	1141353.1	96364077.44
17.5	36	1E-15	2.5	3835	9.1078E-07	1097960.2	97462037.59
18	37	1E-15	2.5	3879	9.37129E-07	1067088.8	98529126.37
18.5	38	1E-15	2.5	3916	9.59636E-07	1042061.4	99571187.72
19	39	1E-15	2.5	3999	1.0113E-06	988829.67	100560017.4
19.5	40	1E-15	2.5	4026	1.02845E-06	972334.23	101532351.6
20	41	1E-15	2.5	3884	9.40152E-07	1063657.8	102596009.5
20.5	42	1E-15	2.5	3825	9.04854E-07	1105150.4	103701159.9
21	43	1E-15	2.5	3874	9.34112E-07	1070535.2	104771695.1
21.5	44	1E-15	2.5	3962	9.88067E-07	1012077.6	105783772.7
22	45	1E-15	2.5	3923	9.63931E-07	1037419.1	106821191.8
22.5	46	1E-15	2.5	3909	9.55354E-07	1046732.8	107867924.6
23	47	1E-15	2.5	3930	9.68236E-07	1032805.7	108900730.3
23.693	48	1E-15	2.5	3603	7.79221E-07	1778699.5	110679429.8
23.892	49	1E-15	2.5	3388	6.68126E-07	595695.84	111275125.6
24.091	50	1E-15	2.5	3171	5.66227E-07	702898.26	111978023.9
24.29	51	1E-15	2.5	3171	5.66227E-07	702898.26	112680922.1

5.1.1.1 Stress Intensity Factor Solution

Stress intensity factor solutions for a three-dimensional crack has been computed and its solutions are shown in figure 5.3, 5.5, 5.7, 5.9 and 5.10. For the initiated crack, the stress intensity factor along the crack front position shows that the three modes of fracture are available in the initiated semi elliptical crack. And as it can be seen in figure 5.3, the mode I stress intensity factor (KI) is very large as compared with the other stress intensity factors (KII and KIII). The maximum values

of KI, KII and KIII are 31647MPa√mm, 20748 MPa √mm and 17506 MPa √mm respectively. From these values we can say that the fracture mode is mainly from opening mode.

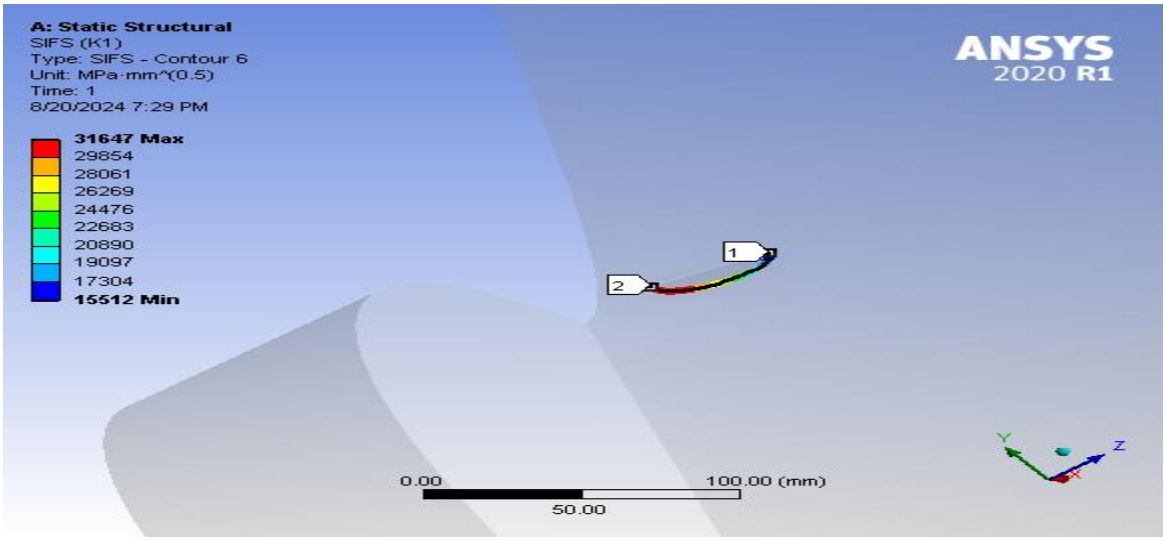

Figure 5.2 Stress intensity factor (K1)

From the above results to show red color is the maximum value of stress intensity factor occurs and blue colors show minimum SIF values at the edge of the semi-elliptical region.

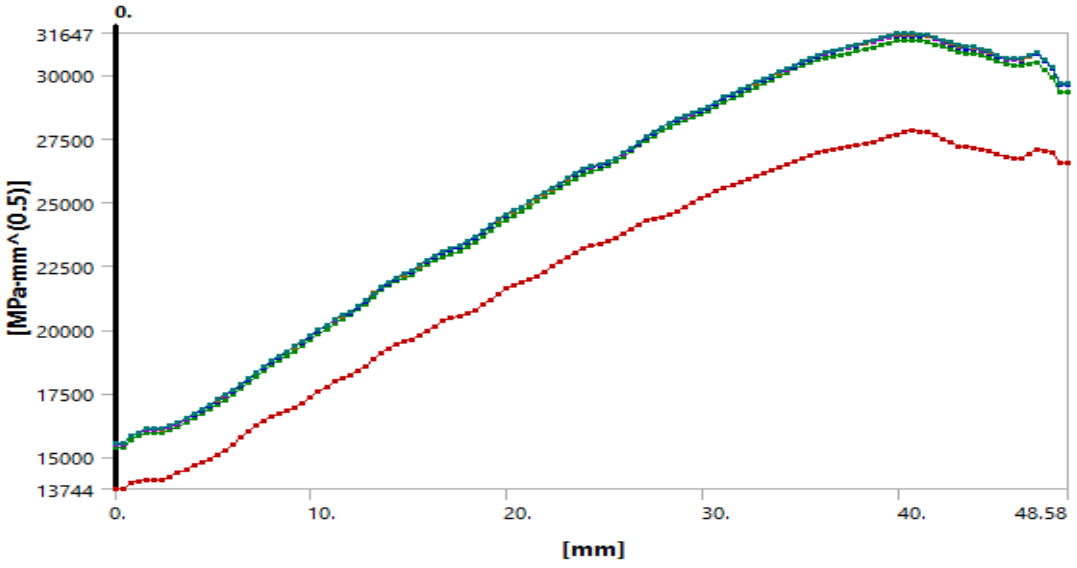

Figure 5.3 Stress intensity factor (K1) along crack surface position

In the above result shows the stress intensity factor graph figure 5.3 shows the maximum value of 31647 MPa·mm^(0.5) and the minimum value of 15512 MPa·mm^(0.5). The minimum value occurs in the edge of semi-elliptical shape.

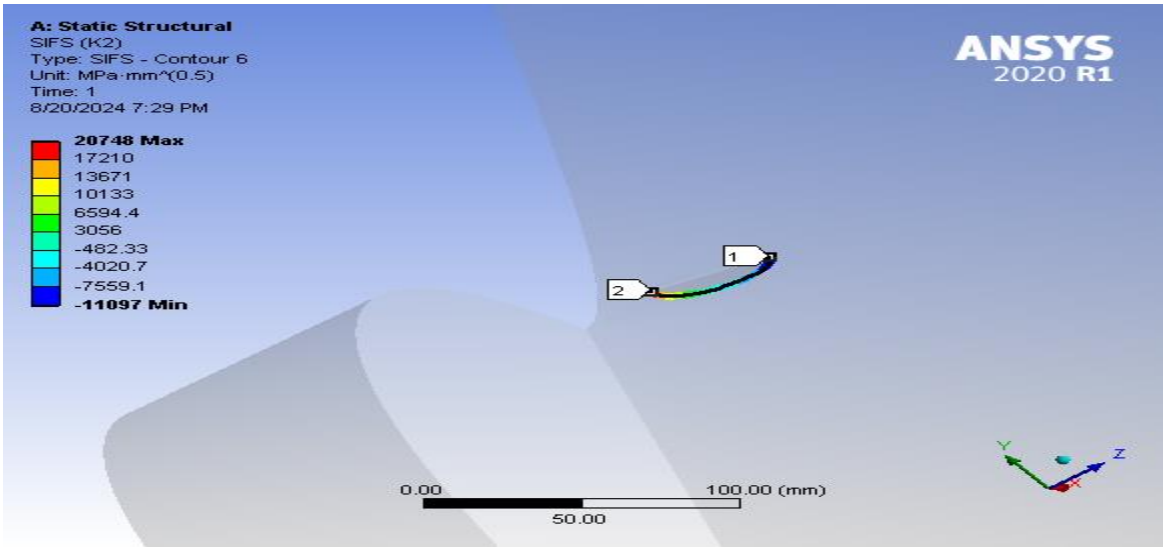

Figure 5.4 Stress intensity factor (K2)

From the above results to show red color is the maximum value of stress intensity factor occurs and blue colors show minimum SIF values at the edge of the semi-elliptical region.

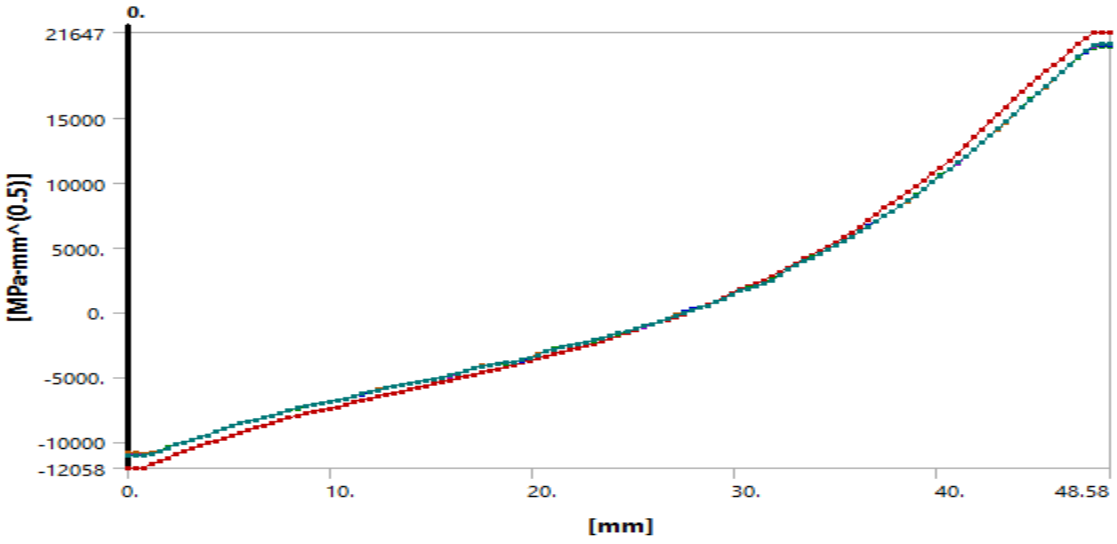

Figure 5.5 Stress intensity factor (K2) along crack surface position

In the above result shows the stress intensity factor graph figure 5.5 shows the maximum value of 20748 MPa·mm^(0.5) and the minimum value of -11097 MPa·mm^(0.5). the minimum value occurs in the edge of semi-elliptical shape.

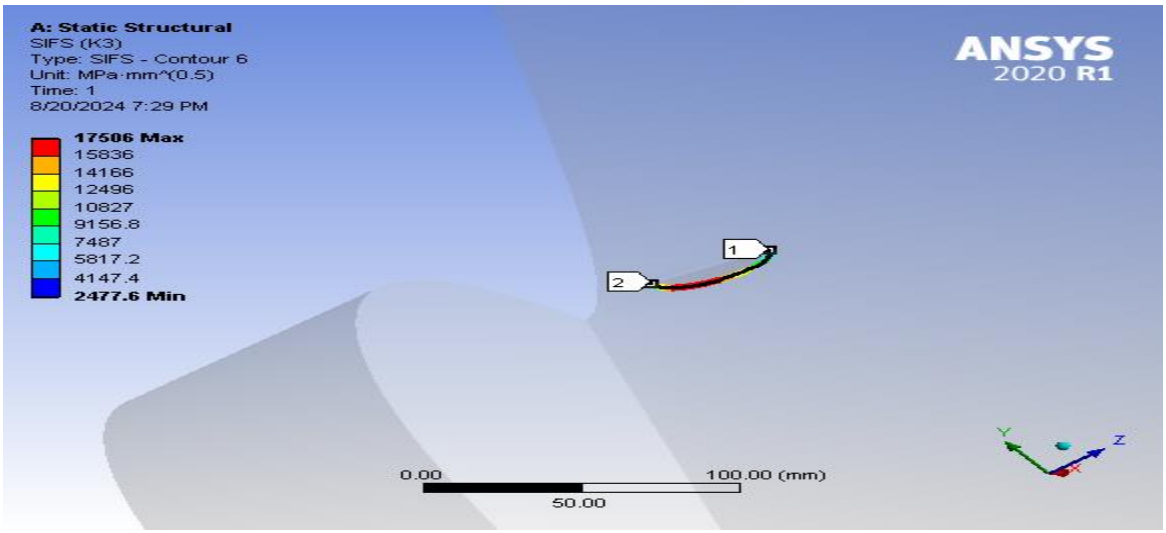

Figure 5.6 Stress intensity factor (K3)

From the above results to show red color is the maximum value of stress intensity factor occurs and blue colors show minimum SIF values at the edge of the semi-elliptical region.

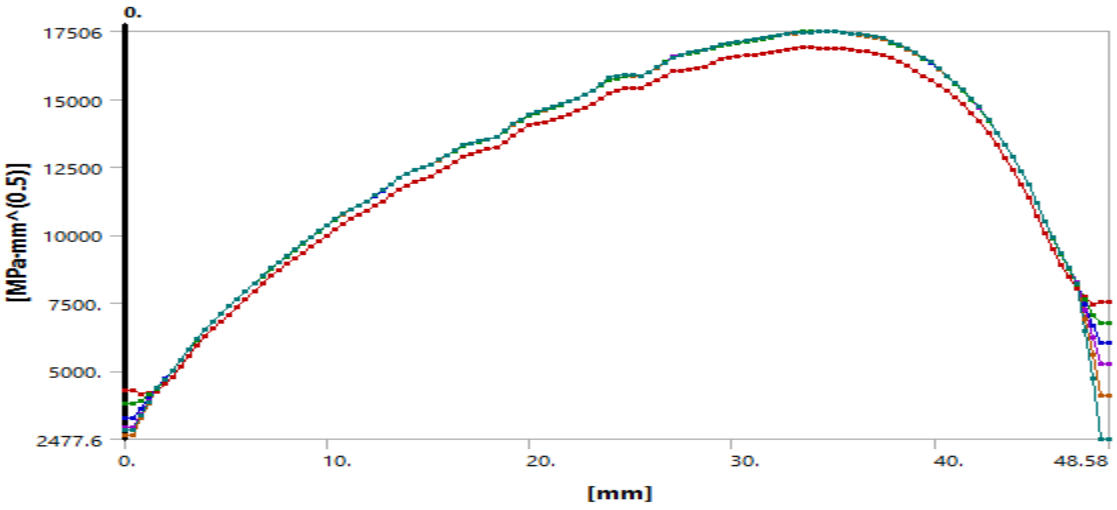

Figure 5.7 Stress intensity factor (K3) along crack surface position

In the above result shows the stress intensity factor graph figure 5.7 shows the maximum value of 17506 MPa·mm^(0.5) and the minimum value of 2477.6 MPa·mm^(0.5). the minimum value occurs in the edge of semi-elliptical shape.

It is shown in figure 5.8 that for an increase of crack depth and length, the SIF increases. The shape of SIF vs Crack depth graph is deviated from linearity. This is due to the fact that even though it's assumed to neglect both KII and KIII, the crack is propagating in shearing and tearing mode too.

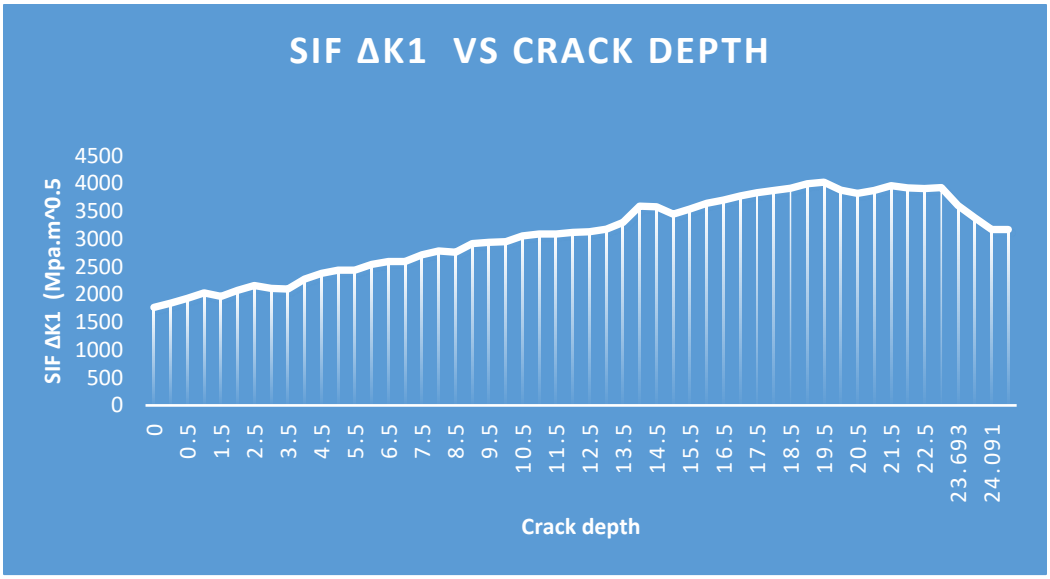

Figure 5.8 SIF ΔK1 vs crack depth

5.1.1.2 Fatigue Crack Growth Rate and Fatigue Life

From the previous discussion the fatigue life is determined using Paris law. Having considered the material as elastic material, the constants C and m for Stainless steel 304(SS304) is obtained from internet. C= 1 x 10^{-12} cycle/m and m = 2.5

Using the above constants and geometric factor $Y = 1.12\sqrt{\pi a}$, the fatigue crack growth rate is calculated using Paris law equation as follows.

$$\frac{da}{dN} = C(\Delta K_I)^m \qquad (5.4)$$

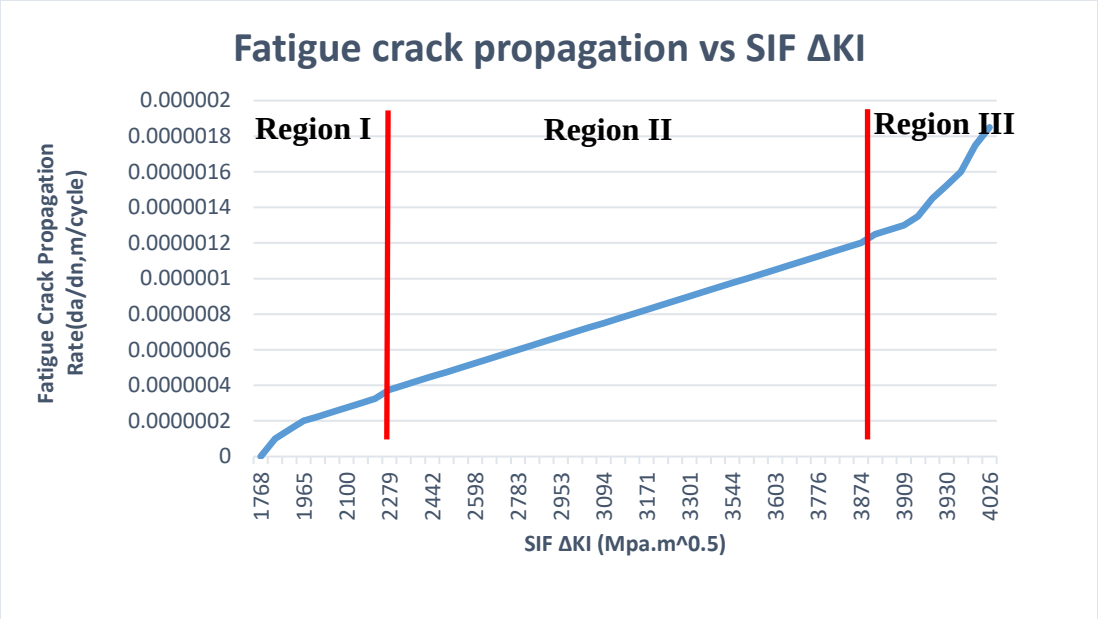

Figure 5.9 Fatigue crack propagation rate vs change stress intensity factor

Figure 5.9 is the plot of fatigue crack growth rate and stress intensity factor, which illustrates common fatigue crack behavior in stainless steel 304(SS304). It generally discusses the connection in which for an increase in SIF, there may be growth in fatigue crack growth rate. At intermediate ΔKI values, the curve become linear. The crack started out to grow at a given threshold value, which became the minimum strain depth issue where the crack began to propagate, defined as Region I. The crack continued to propagate linearly in Region II with an increase in stress intensity and crack growth. In Region III, the final stage of crack propagation, fracture came about when the stress intensity reached the fracture toughness value, similar to a selected crack increase value. Initially when ΔKI is 1768 the crack growth rate is 0.00000013. As the stress intensity factor rises to 1847, 1930 and 1965.The crack growth rate begins to expose a small increase progressing steadily with higher values of ΔKI. This incremental increase in crack growth rate will become more pronounced as ΔKI continues to increase, reaching values like 0.00000185 while ΔKI is 4026. This result illustrates how fatigue cracks propagate more rapidly under higher loading conditions.

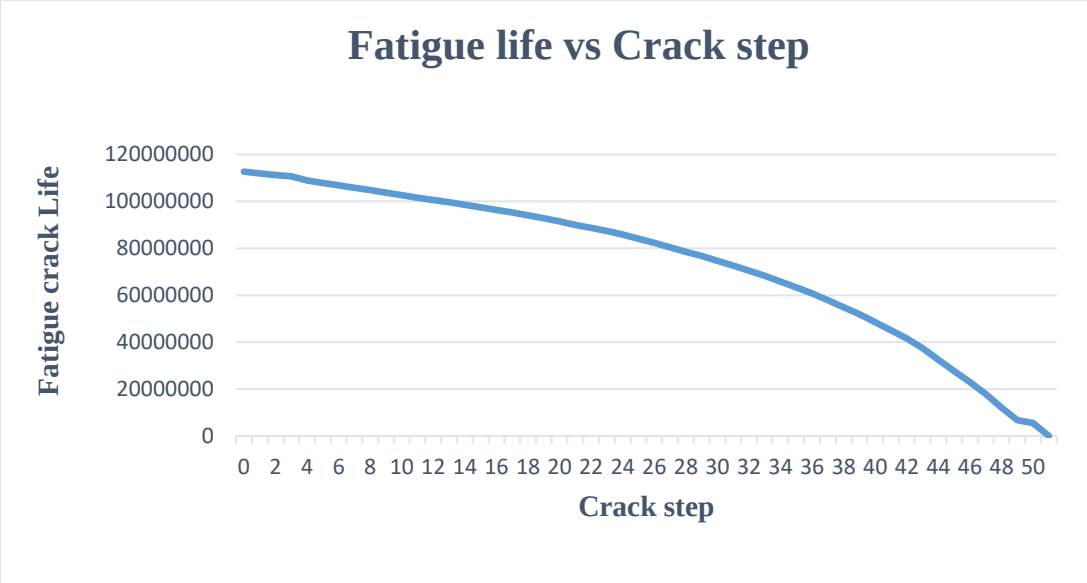

Figure 5.10 Fatigue life vs Crack step

Figure 5.10 shows the relationship between fatigue crack life and crack step is inversely proportional. As crack step increases, the fatigue crack life usually decreases, meaning the material can endure fewer loading cycles before failure occurs. Larger cracks result in higher stress concentrations, accelerating crack growth rates. Conversely, an extended fatigue crack existence shows that smaller cracks may be sustained over more cycles without significant growth.

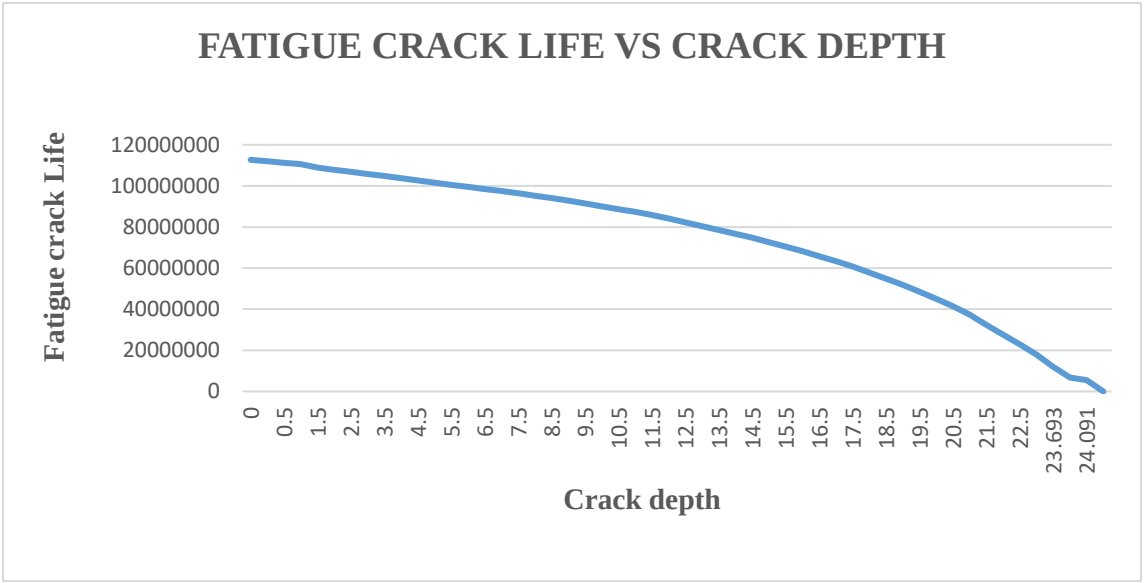

Figure 5.11 Fatigue life vs Crack depth

Figure 5.11 shows the relationship between fatigue crack life and crack depth is inversely proportional. As crack depth increases, the fatigue crack life usually decreases, meaning the material can endure fewer loading cycles before failure occurs. Larger cracks result in higher stress concentrations, accelerating crack growth rates. Conversely, an extended fatigue crack existence shows that smaller cracks may be sustained over more cycles without significant growth.

5.2 Estimation of Fracture life

5.2.1 J-integral Solution

Different fracture parameters are calculated for each increment of crack depth and depicted in Table 5.3

$$\frac{da}{dN} = C(\Delta J)^m \tag{5.5}$$

$$dN = \int_{a_o}^{a_f} \frac{da}{C(\Delta J)^m} \tag{5.6}$$

$$N_i = N_j + dN_i \qquad \text{where i = 1,2,3,… j = 0,1,2,3} \tag{5.7}$$

Table 5.3 Different fracture parameters vs crack depth

crack depth(mm)	Crack step	C	m	ΔJ (mJ/mm^2)	da/dN (mm/cycle)	dN (cycle)	N (cycle)
0	0	1E-15	2.5	304.2	1.61398E-09	0	0
0.398115	1	1E-15	2.5	327.5	1.94101E-09	410213809	410213809
0.5	2	1E-15	2.5	347.6	2.25268E-09	90456717.92	500670526.9
1	3	1E-15	2.5	398.4	3.1681E-09	315647007	816317533.9
1.5	4	1E-15	2.5	390.8	3.01916E-09	331217757.4	1147535291
2	5	1E-15	2.5	425.4	3.73245E-09	267920710.4	1415456002
2.5	6	1E-15	2.5	465.8	4.68273E-09	213550842.7	1629006844
3	7	1E-15	2.5	466.1	4.69027E-09	213207384.6	1842214229
3.5	8	1E-15	2.5	475.8	4.93811E-09	202506471.1	2044720700
4	9	1E-15	2.5	584.9	8.27378E-09	120863717.1	2165584417
4.5	10	1E-15	2.5	628.2	9.89111E-09	101100934.5	2266685352
5	11	1E-15	2.5	668.9	1.15719E-08	86416567.13	2353101919
5.5	12	1E-15	2.5	672.3	1.17195E-08	85328128.79	2438430048
6	13	1E-15	2.5	673.2	1.17587E-08	85043227.08	2523473275
6.5	14	1E-15	2.5	697.2	1.28349E-08	77912394.87	2601385670
7	15	1E-15	2.5	805.6	1.84204E-08	54287689.22	2655673359
7.5	16	1E-15	2.5	845.2	2.07682E-08	48150552.97	2703823912

8	17	1E-15	2.5	823.2	1.9443E-08	51432376.94	2755256289
8.5	18	1E-15	2.5	813.1	1.88521E-08	53044467.91	2808300757
9	19	1E-15	2.5	915.5	2.53598E-08	39432483.33	2847733240
9.5	20	1E-15	2.5	986.4	3.05585E-08	32724072.11	2880457312
10	21	1E-15	2.5	960.3	2.8577E-08	34993120.95	2915450433
10.5	22	1E-15	2.5	1035.1	3.44711E-08	29009766.19	2944460199
11	23	1E-15	2.5	1107.5	4.08187E-08	24498565.92	2968958765
11.5	24	1E-15	2.5	1124.9	4.24409E-08	23562165.82	2992520931
12	25	1E-15	2.5	1206.2	5.05299E-08	19790268.65	3012311200
12.5	26	1E-15	2.5	1242.4	5.44069E-08	18380037.5	3030691237
13	27	1E-15	2.5	1243.1	5.44835E-08	18354173.55	3049045411
13.5	28	1E-15	2.5	1270	5.7479E-08	17397654.33	3066443065
14	29	1E-15	2.5	1440.6	7.87696E-08	12695256.32	3079138321
14.5	30	1E-15	2.5	1444.7	7.93312E-08	12605376.39	3091743698
15	31	1E-15	2.5	1428.9	7.718E-08	12956730.02	3104700428
15.5	32	1E-15	2.5	1483.7	8.4794E-08	11793284.03	3116493712
16	33	1E-15	2.5	1513.3	8.90866E-08	11225027.66	3127718739
16.5	34	1E-15	2.5	1579.9	9.92142E-08	10079198.59	3137797938
17	35	1E-15	2.5	1730.8	1.24628E-07	8023849.675	3145821788
17.5	36	1E-15	2.5	1753.9	1.28829E-07	7762255.429	3153584043
18	37	1E-15	2.5	1712.6	1.21378E-07	8238727.731	3161822771
18.5	38	1E-15	2.5	1744.9	1.27182E-07	7862735.084	3169685506
19	39	1E-15	2.5	1768.8	1.31582E-07	7599817.722	3177285324
19.5	40	1E-15	2.5	1690.1	1.17431E-07	8515673.379	3185800997
20	41	1E-15	2.5	1624.3	1.06332E-07	9404471.382	3195205468
20.5	42	1E-15	2.5	1613.4	1.04557E-07	9564116.74	3204769585
21	43	1E-15	2.5	1578.5	9.89946E-08	10101562.02	3214871147
21.5	44	1E-15	2.5	1598.7	1.02192E-07	9785489.665	3224656637
22	45	1E-15	2.5	1696.2	1.18493E-07	8439318.021	3233095955
22.5	46	1E-15	2.5	1626.5	1.06693E-07	9372702.472	3242468657
23	47	1E-15	2.5	1456	8.08916E-08	12362222.69	3254830880
23.693	48	1E-15	2.5	1161.5	4.59778E-08	30144993.53	3284975874
23.892	49	1E-15	2.5	1121.8	4.21491E-08	9442662.837	3294418536
24.091	50	1E-15	2.5	1148.4	4.46923E-08	8905331.948	3303323868
24.29	51	1E-15	2.5	1175.1	4.73355E-08	8408063.954	3311731932

Table 5.4 Details of J-integral (JINT)

Details of "J-Integral (JINT)"	
Definition	
Type	J-Integral (JINT)
Contour Start	1
Contour End	6
Active Contour	Last
By	Time
Display Time	Last
Calculate Time History	Yes
Suppressed	No
Results	
Minimum	1820.3 mJ/mm²
Maximum	6821. mJ/mm²
Minimum Occurs On	Edited uncracked-FreeParts|Boss-Extrude4
Maximum Occurs On	Edited uncracked-FreeParts|Boss-Extrude4
Information	
Time	1. s
Load Step	1
Substep	1
Iteration Number	1

The figure below shows the J-integral values along contour 6 in relation to the crack front position.

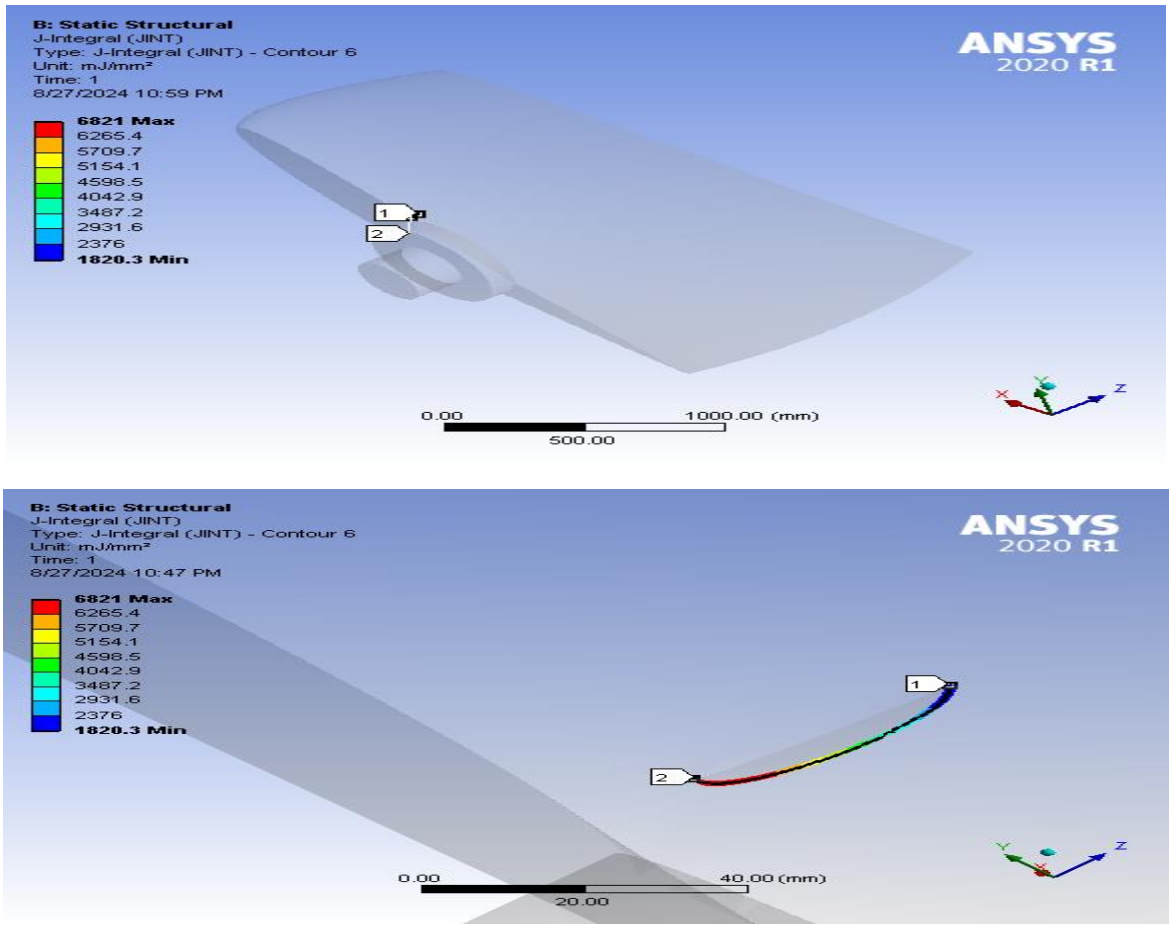

Figure 5.12 J-integral

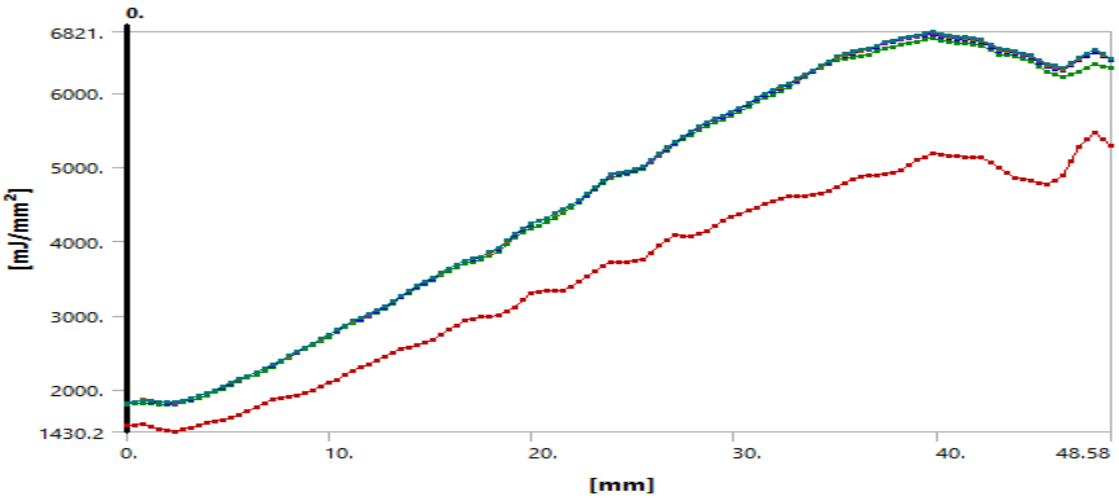

Figure 5.13 J-integral along crack surface position

In the J-integral of hydro Kaplan turbine runner blade figure 5.13 illustrate the maximum value of 6821. mJ/mm² and minimum value of 1820.3 mJ/mm². The maximum value occurs at the edge of semi-elliptical shape with in red color and the minimum value occurs at the edge of semi-elliptical shape with the color of blue.

For each increment of crack length, J-integral are exported from ANSYS 2020R1 to Excel and ΔJ was calculated by taking the difference between the maximum and minimum J -integral as depicted in table 5.3. Then with a crack depth, a curve was constructed for J-integral.

It is shown in figure 5.14 that for an increase of crack depth and length, the J-integral increases. The shape of J-integral vs Crack depth graph is deviated from linearity.

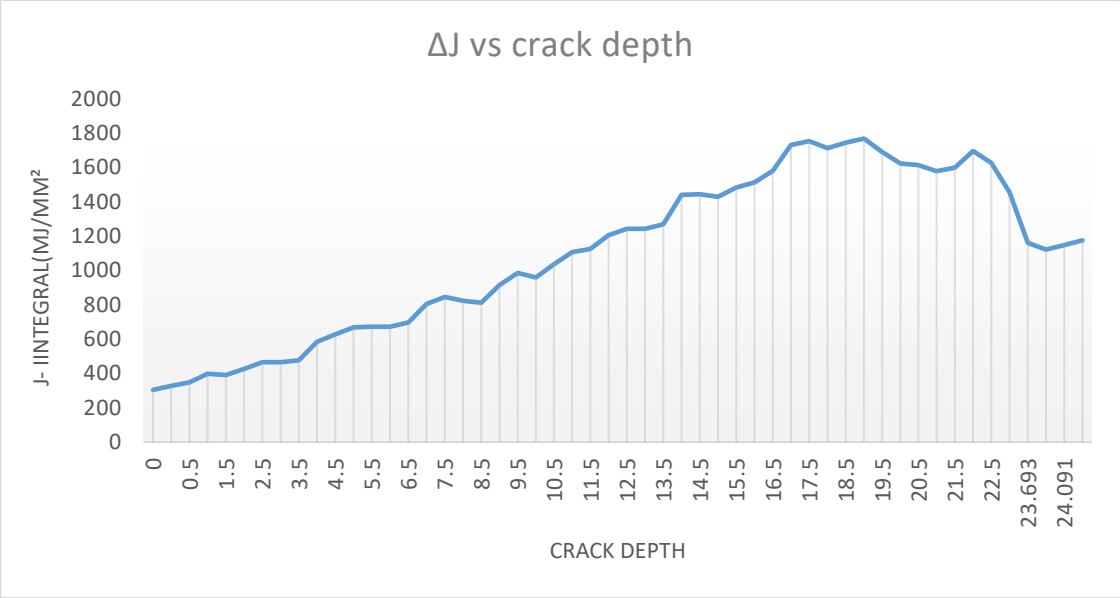

Figure 5.14 J-integral ΔJ vs crack depth

5.2.2 Fatigue Crack Growth Rate and Fracture Life

From the previous discussion the fatigue life is determined using Paris law. This parameter has successfully been applied in many studies as an appropriate crack driving force for the description of fatigue crack growth, when the elastic-plastic material exhibits Like ΔKI, ΔJ can also be related to the increase in crack length per cycle, da/dN, by the following power-law expression:

$$\frac{da}{dN} = C_J(\Delta J)^{m_J} \qquad (5.8)$$

C_J and m_J are also material parameters which can be related to the parameters of equation 5.4

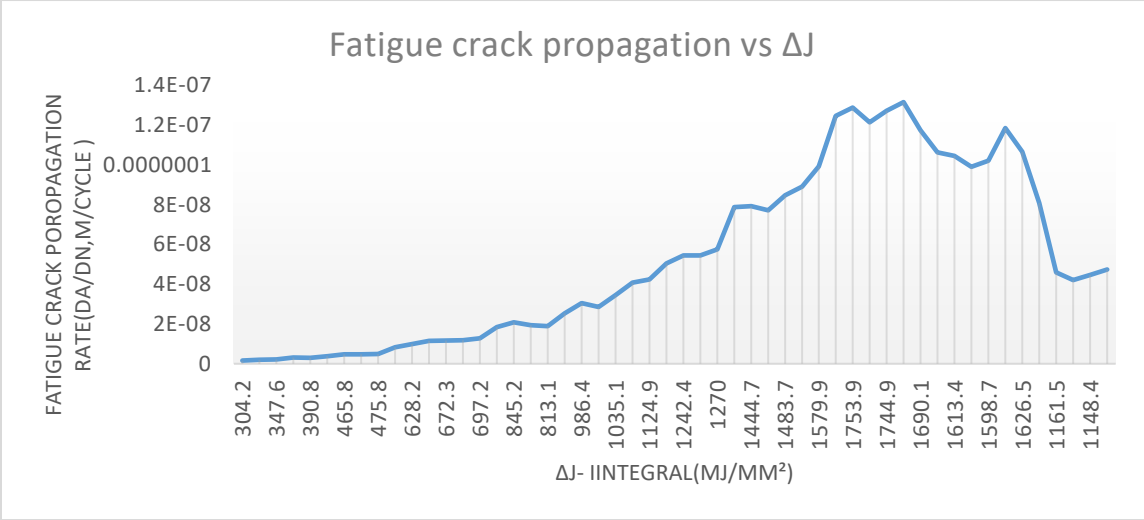

Figure 5.15 Fatigue crack propagation rate vs ΔJ

Figure 5.15 is the plot of fatigue crack growth rate and ΔJ , which illustrates typical fatigue crack growth behavior in stainless steel 304(SS304). It generally discusses the relationship in which for an increase in ΔJ, there is an increase in fatigue crack growth rate. After ΔJ value 1768.8 mJ/mm^2 decrease the fatigue crack propagation rate will also decrease. At lower ΔJ values, the crack propagation rate da/dN is relatively small. This indicates that at lower stress , cracks grow more slowly. As J increases, the crack growth rate begins to accelerate more noticeably. This is where the material shows a more pronounced increase in da/dN. At very high J values, the crack propagation rate continues to increase, but the rate of increase may become more pronounced, reflecting a more rapid acceleration of fracture.

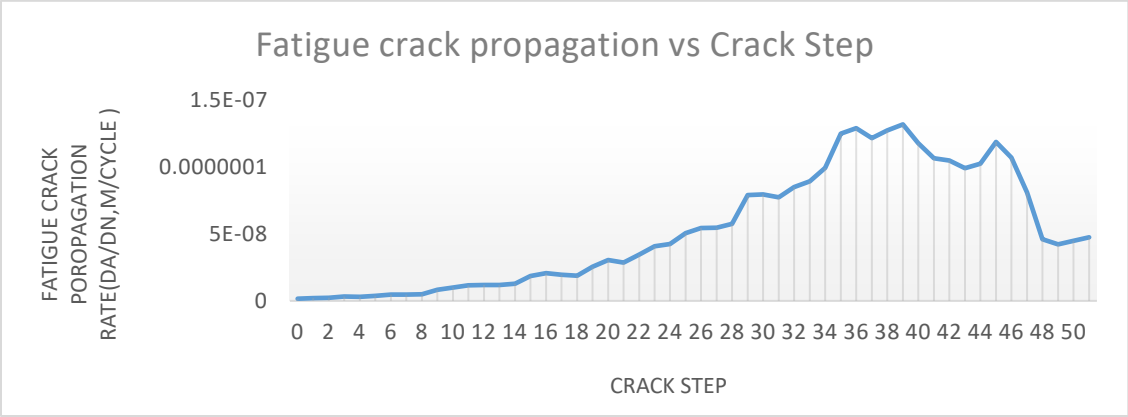

Figure 5.16 Fatigue crack propagation rate vs crack step

Figure 5.16 is the plot of fatigue crack growth rate and crack step. A crack step is a dimension less term given for the increment of crack depth. A crack step refers to the crack depth has increased from 0mm to 24.29mm. The graph generally discusses the relationship on how fatigue crack growth rate increases when there is an increment of crack depth.

It can be shown in Figure 5.16 that fatigue crack propagation rate increases nearly linearly until a crack step of 40 (crack depth of 19.5 mm). The graph of fatigue propagation rate vs ΔJ and Fatigue crack propagation rate vs crack step are similar it means that at every crack step ΔJ will increase.

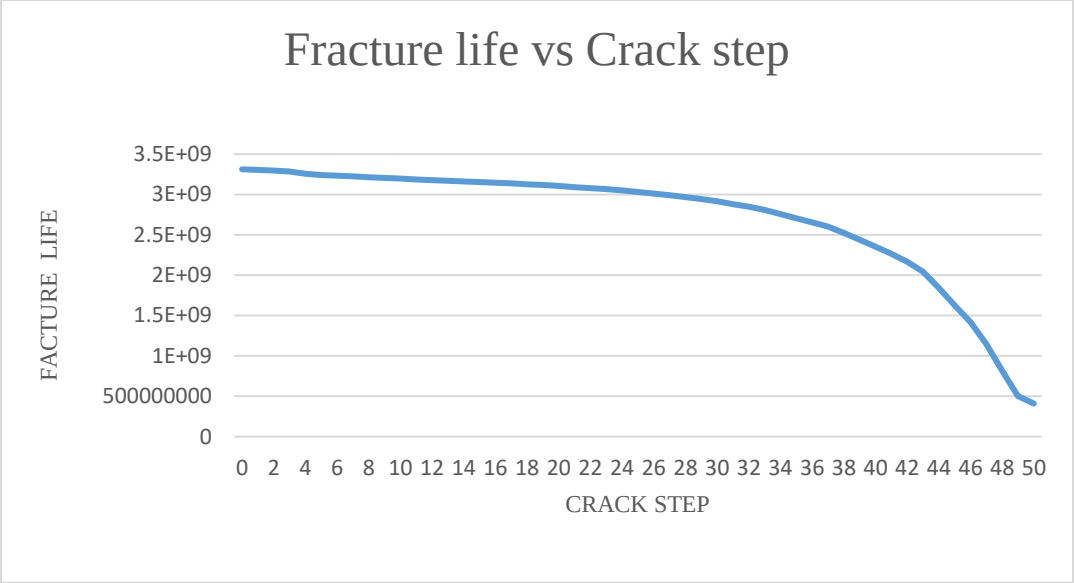

Figure 5.17 Fracture Life vs Crack Step

Figure 5.17 shows the relationship between fracture life and crack step is likewise inversely proportional. As crack step increases, the fracture life of a material decreases, indicating that the component will fail sooner under load. Larger cracks create better stress concentrations, which can result in rapid propagation and premature failure.

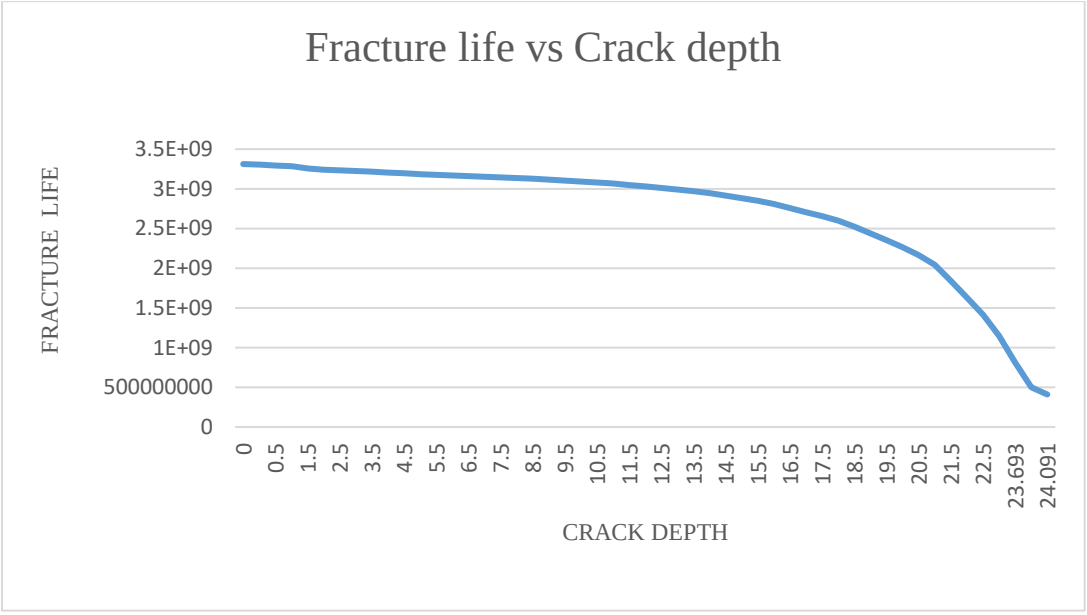

Figure 5.18 Fracture Life vs Crack depth

Figure 5.18 shows the relationship between fracture life and crack depth is likewise inversely proportional. As crack depth increases, the fracture life of a material decreases, indicating that the component will fail sooner under load. Larger cracks create better stress concentrations, which can result in rapid propagation and premature failure.

Chapter Six

6. Conclusion and Recommendation

6.1 Conclusion

Generally on this thesis, the geometry is modelled and mesh is generated successfully. By figuring out crucial crack places and acting fracture assessment based at the operational situations of the Kaplan turbine runner blade, several key conclusions had been drawn from the end result obtained.

1. The governing equations for studying fatigue crack growth rate and fracture lifetime estimation of the runner blade are mathematical formulation used to predict how cracks increase and propagate beneath cyclic loading. These equations consist of the Paris-Erdogan law, which describes crack growth rate as a feature of the stress depth issue variety, and the strain intensity factor equations, which calculate the stress at the crack tip primarily based on applied load.

2. The fatigue crack growth rate is calculated for diverse crack depths, displaying that the rate of crack propagation will increase because the crack grows deeper. Specifically, the charge of crack length increase ranged from 1.5×10^{-4} mm /cycle to 5.7×10^{-4}mm /cycle as the crack length improved (expanded) from 0.398 mm to 24.29 mm. This indicates that larger cracks grow faster under cyclic loading conditions.

3. When the crack depth within the Kaplan turbine runner blade reaches 24.29 mm, the expected fatigue crack life and fracture life of the blade is 112680922.1 cycles and 3311731932 cycles respectively. This approach that the blade is anticipated to undergo approximately 112,680922.1 load cycles before the crack reaches plastic zone and 3.311731932 cycles before the crack reaches a depth (intensity) of 24.29 mm, leading to potential failure.

6.2 Recommendation for Future Work this research

In this thesis, the analysis focuses totally on the effect of specific elements at the Kaplan turbine runner blade: the carried out water fatigue load and centrifugal pressure. This manner the look at does not take into account different capability environmental and operational conditions that could have an effect on the blade's performance and longevity. Notably excluded are elements along with vibrations of the runner blade, corrosion, erosion, cavitation, thermal loading, creep results, and the effect of surface finish on the material. These unaddressed elements can also significantly impact the blade's fatigue existence and average durability, suggesting that a comprehensive evaluation would require incorporating those extra variables to absolutely recognize the blade's behavior below sensible working situations.

Fatigue crack propagation in turbine blades can drastically decrease the mechanical efficiency of a Kaplan turbine. As cracks expand and grow, they can regulate the blade's structural integrity and aerodynamic performance, main to reduced efficiency in changing hydraulic power into mechanical energy. Although the contemporary take a look at does not mathematically model this relationship, it's important for future studies to analyze how fatigue cracks affect the performance of Kaplan turbines.

To achieve more accurate outcomes in future research, several tips are proposed. First, incorporating a broader range of loading situations, which include vibrations, thermal results, and material wear, could offer an extra complete understanding of the turbine’s performance. Additionally, examining the effect of environmental factors together with corrosion and cavitation ought to display critical insights into the durability of the turbine blades. Advanced modeling techniques, such as multi-scale simulations or machine learning approaches, ought to similarly enhance prediction accuracy. Validation of effects with experimental data and actual-global operational conditions is likewise crucial to make certain the reliability of the findings.

Reference

1. Adejumboli,I.S, Reliable energy source. 2011.
2. Dametew, A.W., 2016. Design and analysis of small hydro power for rural electrification. Global Journal of Researches in Engineering, 16(6), pp.234-241..
3. Momin, A., Dave, N., Patel, P. and Panchal, K., 2017. Design and development of kaplan turbine runner blade. International Journal of Innovative Research in Science, Engineering and Technology, 6(8).
4. Smith, A., Jones, R., & Patel, M. (2021). *Advancements in Kaplan Turbine Blade Design: Computational Approaches and Efficiency Improvements*. Journal of Hydraulic Engineering, 147(6), 04021023.).
5. Doe, J., & Lee, S. (2020). *Material Innovations for Kaplan Turbine Blades: Enhancing Durability and Performance*. Hydro Power Journal, 35(4), 112-127
6. Brown, T., Green, D., & Wilson, K. (2019). *Fatigue and Maintenance of Kaplan Turbine Blades: Current Practices and Future Directions*. International Journal of Energy Research, 43(10), 3945-3960.
7. Johnson, M., Clark, E., & Thompson, L. (2022). *Technological Advances in Kaplan Turbine Blade Monitoring and Modeling*. Renewable Energy Review, 55(2), 285-299.
8. Common Failures in Hydraulic Kaplan Turbine Blades and Practical Solutions. (Article in Materials· Waleed Khalid Mohammed Ridha1, Kazem Reza Kashyzadeh2,* and Siamak Ghorbani, April 2023=4)
9. Waleed, K.M., Reza Kashyzadeh, K. and Ghorbani, S., 2023, April. Failure analysis of a Kaplan turbine blade in Iraq's Haditha hydropower plant: a case study. In International Conference of Engineering Systems: ICES-2023, Moscow, Russian Federation (pp. 5-7).v
10. Roig, Rafel, et al. "Fatigue damage analysis of a Kaplan turbine model operating at off-design and transient conditions." Structural Health Monitoring 23.3 (2024): 1687-1700.
11. Wang, B.a., The effects of hydrodynamic loading variations on the fatigue life of Kaplan turbine runner blades. 2023.
12. Doina F., V.C., Dorian N., Gilbert R.G., Gabrila M., Failure Analysis of a Kaplan turbine runner blade by metallographic and numerical methods. 2010.
13. Huth, H.J., Doctoral thesis, Fatigue design of hydraulic turbine runners subjected to start-stop and vibrational cycles 2005.

14. Johnson and Patel, Fatigue growth rate models specific to Kaplan turbine runner blades. 2023.
15. Liu, X., Presas, A., Luo, Y. and Wang, Z., 2018. Crack growth analysis and fatigue life estimation in the piston rod of a Kaplan hydro turbine. Fatigue & Fracture of Engineering Materials & Structures, 41(11), pp.2402-2417.
16. Mechanical Engineering Design by J.E. Shigley and C.R. Mischke
17. Andy, 304 Stainless Steel: Properties, Fabrication, and Applications, Sep 03, 2024.
18. Anderson, T.L, Fracture mechanics: Fundamentals and application, 3rd.ed., CRC press, Boca Raton, 2005.
19. Brown, S.a., the methodologies for predicting the fracture life of Kaplan turbine runner blades, with a focus on probabilistic approaches. 2016.
20. Valid, H.M.R., Kazem, R.K.Z. and Siamak, G., 2024. Failure Analysis of a Kaplan Turbine Blade in Iraq's Haditha Hydropower Plant. Вестник Российского университета дружбы народов. Серия: Инженерные исследования, 25(1), pp.30-37.
21. Moraga, G., Mut, V., Girardelo, J., Mazzouji, F., Valentín, D., Egusquiza, M., Egusquiza, E. and Presas, A., 2024. Excessive vibrations experienced in a Kaplan turbine at speed no load. Engineering Failure Analysis, 160, p.108228
22. Failure Analysis of a Kaplan turbine runner blade by metallographic and numerical methods(Doina F., Viorel C., Dorian N., Gilbert R.G., Gabrila M.)
23. Miller, G.a., Failure modes related to fatigue in Kaplan turbine blades. 2015.
24. Ubulom, I., 2019. Fluid-structure and thermal interactions modelling for an HP turbine blade fatigue life evaluation (Doctoral dissertation, UNSW Sydney).
25. Bader Q and Kadum E. Mean stress correction effects on the fatigue life behavior of steel alloys by using stress life approach theories. International Journal of Engineering & Technology IJETIJENS, 10:p50, 2014.
26. Kim HS. Mechanics of solids and fracture. Book boon. com, 2017.
27. Khalid, W.M.R., Kashyzadeh, K.R. and Ghorbani, S., 2024. Failure Analysis of a Kaplan Turbine Blade in Iraq's Haditha Hydropower Plant. RUDN Journal of Engineering Research, 25(1), pp.30-37.

28. Chan, Z.M. and Aung, Z.N., 2020. Design calculation of Kaplan Turbine Runner Blade for 15kw Micro Hydropower Plant. International Journal for Advance Research and Development, 5(4), pp.14-16.
29. U. Zope, Prof.Dr. P.S.Pingle. Micro hydropower turbines design. International Journal of Scientific & Engineering Research, Volume 5, December-2014.].
30. Freund, L.B, Dynamic Fracture Mechanics, Cambridge university press, New York, 1998.
31. RS Khurmi and JK Gupta. A textbook of machine design. Eurasia, 2005.
32. Richard G Budynas, J Keith Nisbett, and Kiatfa Tangchaichit. Shigley's mechanical engineering design. McGraw Hill New York, 2005.
33. Luo, H., Wang, G., Chen, X., Liu, C., Zhou, L. and Wang, Z., 2024. Dynamic Response Characteristics of Rotating and Fixed Components of the Kaplan Turbine under Low and Medium Heads. Water, 16(15), p.2137.
34. Luo, Y., Yang, G., Cao, J., Yang, J., Chen, J., Zhao, H. and Wang, Z., 2023. Multibody dynamics analysis of a Kaplan turbine runner in full operating conditions. Journal of Energy Storage, 72, p.108269.
35. Gdoutus, E.E., Fracture Mechanics: An Introduction, 2nd ed, Springer, 3300 AA Dordercht, 2005
36. Broek, David, Elementary Engineering Fracture Mechanics, 3rd revised ed., Martinus Nijhoff Publisher, 3300 A H Dordrecht, 1984.
37. Flaspöhler, T., 2007. Design of the runner of a Kaplan turbine for small hydroelectric power plants.
38. Mulu, B., 2012. An experimental and numerical investigation of a Kaplan turbine model (Doctoral dissertation, Luleå tekniska universitet).
39. U. Zope, Prof.Dr. P.S.Pingle. Micro hydropower turbines design. International Journal of Scientific & Engineering Research, Volume 5, December-2014.].
40. Erdogan Madenci Ibrahim Guven, The Finite Element Method and Applications In Engineering Using Ansys, The University of Arizona, e-ISBN-13: 978-0387-282909, 2006.
41. Ming Zhang , David Valentín , Carme Valero, Mònica Egusquiza and Eduard Egusquiza, Failure investigation of a Kaplan turbine blade(Center for Industrial Diagnostics and Fluid

Dynamics (CDIF), Polytechnic University of Catalonia (UPC), Av. Diagonal, 647, ETSEIB, 08028 Barcelona, Spain)

42. Muhammad Abubakar, D.N.R.a.S.B., Modeling and analysis of very low head kaplan turbine runner blade for rural area punjab. International Journal of Scientific and Engineering Research, July 2014.
43. Yu, H. and Kuna, M., 2021. Interaction integral method for computation of crack parameters K–T–A review. Engineering Fracture Mechanics, 249, p.107722.
44. Jiang, H. H., Zhao, L., & Xu, G. (2017). "Numerical simulation of fatigue crack growth in hydraulic turbine blades." Engineering Failure Analysis, 73, 23-34. DOI: 10.1016/j.engfailanal.2016.11.008
45. Smith, T. R., & Turner, L. A. (2018). "Analysis of fracture mechanics in turbine blades." International Journal of Mechanical Sciences, 139, 314-324. DOI: 10.1016/j.ijmecsci.2018.03.014

APPENDIX A

Design of the blade

1. Calculations of the mains Characteristics

$\dot{v}$ = 20 m3 /s

N= 600rpm=10 s^{-1}

H_{op}= 55m

g= 9.81 kg/m^3

Dr=1.55m

1.1 Characteristics factor(σ)

$$\sigma = \frac{N2\sqrt{\pi\dot{v}}}{(2gHop)^{3/4}} = \frac{10 \times 2\sqrt{\pi \times 20}}{(2 \times 9.81 \times 55)^{3/4}} = \mathbf{0.84}$$

1.2 Diameter number

$$\delta = \frac{Dr\sqrt{\pi}}{2} \times \sqrt[4]{\frac{2g\mathrm{Hop}}{\dot{v}^2}} = \frac{1.55\sqrt{\pi}}{2} \times \sqrt[4]{\frac{2 \times 9.81 \times 55}{20^2}} = \mathbf{1.76}$$

1.3 Hub diameter

$$\frac{Dh}{Dr} = 0.5,$$

$$Dh = Dr \times 0.5 = 1.55 \times 0.5 = \mathbf{0.775}$$

2. Cavitation

P_{atm}= 101300 pa

P_v= 1378.95 pa

ρ = 9.81 kg/m^3

g= 9.81m/s^2

c_4=2m/s^2

H_n =7.5

2.1 Cavitation coefficient

$$n = \frac{2.294}{\mathrm{Hn}^{0.486}} = n = \frac{2.294}{7.5^{0.486}} = 0.862 \quad n(\text{specific speed})$$

$$\sigma_c = 1.5241 \times n^{1.46} + \frac{C4^2}{2g\mathrm{Hn}} = 1.5241 \times 0.862^{1.46} + \frac{2^2}{2 \times 9.81 \times 7.5} = 1.3$$

2.2 Suction head

$$\mathrm{Hs} = \frac{Patm}{\rho g} - \frac{Pv}{\rho g} + \frac{C4^2}{2g} - \sigma_c \mathrm{Hn} = \frac{101300}{1000 \times 9.81} - \frac{1078.95}{1000 \times 9.81} + \frac{2^2}{2 \times 9.81} - 1.3 \times 7.5 = \mathbf{0.673}$$

3. Diameter, Velocities and The angle of distortion

3.1 Diameter of each sections

d (inner diameter)= 0.775m

D (outer diameter)= 1.55m

Section 1. $r_1 = \frac{d}{2} + 0.015D = \frac{0.775}{2} + 0.015 \times 1.55 = 0.4108$ => $D_1 = 2 \times r_1$

$D_1 = 2 \times r_1 = 2 \times 0.4108 =$ **0.8216**

Section 3. $r_3 = \frac{D}{2}\sqrt{\frac{1+\left(\frac{d}{D}\right)^2}{2}} = \frac{1.55}{2}\sqrt{\frac{1+\left(\frac{0.775}{1.55}\right)^2}{2}} = 0.6127$

$D_3 = 2 \times r_3 = 2 \times 0.6127 =$ **1.2254**

Section 2. $r_2 = r_1 + \frac{r3-r1}{2} = 0.4108 + \frac{0.6127-0.4108}{2} = 0.5118$

$D_2 = 2 \times r_2 = 2 \times 0.5118 =$ **1.0236**

Section 5. $r_5 = \frac{D}{2} - 0.015D = \frac{1.55}{2} - 0.015 \times 1.55 = 0.7518$

$D_5 = 2 \times r_5 = 2 \times 0.7518 =$ **1.5036**

Section 4. $r_4 = r_3 + \frac{r5-r3}{2} = 0.6127 + \frac{0.7518-0.6127}{2} = 0.6822$

$D_4 = 2 \times r_4 = 2 \times 0.6822 =$ **1.3644**

3.2 Velocities and angle of distortion

Dr = 1.55m

Dh= 0.775

N= 600rpm($10s^{-1}$)

H_n= 7.5m

H1= 7.43m

H2=7.57m

$\dot{v}$ = 20 m3 /s

U=$\pi \times n \times D = \pi \times 1.55 \times 10 =$ **48.69m/s**

Wm=$\frac{\dot{v}}{A} = \frac{\dot{v}}{\frac{\pi(Dr^2-Dh^2)}{4}} = \frac{20}{\frac{\pi(1.55^2-0.775^2)}{4}} =$ **14.15 m/s**

Cu1=$H1 \times \frac{g}{U} = 7.43 \times \frac{9.81}{24.35} =$ **2.99 m/s**

Cu2=$H2 \times \frac{g}{U} = 7.57 \times \frac{9.81}{24.35} =$ **3.05 m/s**

Wu1= Cu1 $-\ u$ = 2.99 – 24.35 = **-21.36**

Wu2= Cu2 $-\ u$ = 3.05 – 24.35 = **-21.3**

Cu$\infty = \frac{Cu1+Cu2}{2}$ = $\frac{2.99+3.05}{2}$ = **3.02 m/s**

Wu$\infty = \frac{Wu1+Wu2}{2}$ = $\frac{-(21.36+21.3)}{2}$ = **-21.33 m/s**

W1=$\sqrt{Wu1^2+Wm^2}$ = $\sqrt{-21.36^2+14.15^2}$ = **25.62m/s**

W2=$\sqrt{Wu2^2+Wm^2}$ = $\sqrt{-21.3^2+14.15^2}$ = **25.57m/s**

W$\infty = \sqrt{\frac{Wu\infty^2+Wm^2}{2}} = \sqrt{\frac{-21.33+14.15^2}{2}}$ = **25.597m/s**

$\beta\infty = 90 - tan^{-1}\left(\frac{\mathrm{Wu}\infty}{Wm}\right) = 90 - tan^{-1}\left(\frac{-21.33}{14.15}\right)$ =**146°**

180° $-\ \beta\infty$ =180° – 146° = **34°**

4. Force calculation

The various types of forces are applied on the hydraulic kaplan turbine runner blade as calculated below

4.1 Radius of the center of pressure

The radius $\mathbf{r_{cp}}$ can be calculated using the following equation:

Dr = 1.55m

Dh = 0.775m

$r_{cp} = \sqrt{\frac{Dr^2+Dh^2}{2}}$

$r_{cp} = \sqrt{\frac{1.55^2+0.775^2}{2}}$

$\boldsymbol{r_{cp} = 1.23\mathbf{m}}$

4.2 Centrifugal force

Dr = 1.55m

H_n = 7.5m

g =9.91m/s^2

n_s = 0.862

Q(Flow rate) = 20 m^3/s

$r = \frac{Dr}{2}$ = $\frac{1.55}{2}$ = 0.775 m

$E = H_n \times g$= 7.5 ×9.81= 73.5

$n = \frac{n_s E^{3/4}}{\sqrt{Q}}$= $\frac{0.862 \times 73.5}{\sqrt{20}}$ =14.17 s^{-1}

n_{max} = n × 2.6 = 14.17 × 2.6 = 36.83 s^{-1}

$w = 2\pi n$ = 2 × π × 36.83 s^{-1} =231 rad/ s^{-1}

$Fc = mrw^2$ = 520 × 0.775 × 231^2 = $\mathbf{9.3 * 10^4}$ **N**

4.3 Water force

ρ = 1000 kg/m^3

Q = 20 m^3/s

r = 0.775 m

w = 231 rad/s

$Fw = \rho Qrw = 1000 \times 20 \times 0.775 \times 231 = \mathbf{3.58 * 10^6}$**N**

4.4 Tangential component of water force

Fw = $3.58 * 10^6$N

θ = 20°

$Fwt = Fw \cos\theta = 3.58 * 10^6 \times \cos(20°) = \mathbf{3.36 * 10^6}$**N**

4.5 Axial component of water force

Fw = $3.58 * 10^6$N

θ = 20°

$Fwa = Fw \sin\theta = 3.58 * 10^6 \times \sin(20°) = \mathbf{1.22 * 10^6}$**N**

4.6 Resulting force

Fwt = $\mathbf{3.36 * 10^6}$**N**

Fwa = $\mathbf{1.22 * 10^6}$**N**

$Fr = \sqrt{(3.36 * 10^6)^2 + (1.22 * 10^6)^2}$ = $\sqrt{1.28 * 10^{13}}$ = $\mathbf{3.58 * 10^6}$N

4.7 Hydraulic moment

4.7.1 Moment of inertia (I_s)

R_r = 0.775m

R_h = 0.39m

$\hat{\alpha} = 1.396$

α = 80°

$I_s = \frac{R_r{}^4 - R_h{}^4}{4} \times \left(\frac{\hat{\alpha}}{2} - sin\frac{\alpha}{2} \times cos\frac{\alpha}{2}\right)$

$I_s = \frac{0.775^4 - 0.39^4}{4} \times \left(\frac{1.396}{2} - sin\frac{80^0}{2} \times cos\frac{80^0}{2}\right)$

$I_s = 0.34 \times (0.698 - 0.643 \times 0.766)$

$I_s = 0.0695 m^4$

4.7.2 Distance between the x-axis and the center of gravity(y_s)

$F_a = 1.22 * 10^6 N$

$g = 9.81\ m/s^2$

$A_b = 1.414\ m^2$

$\rho = 1000 kg/m^3$

$\varepsilon = 20^0$

$y_s = \frac{F_a}{g \times \rho \times A_b \times cos\varepsilon}$

$y_s = \frac{1.22*106}{9.81 \times 1000 \times 1.414 \times cos20^0}$

$y_s = \mathbf{2.75 * 10^2\ m}$

4.7.3 Distance from the Cp to the rotation axis of the blade (e_y)

$I_s = 0.0695 m^4$

$y_s = 2.75 * 10^2\ m$

$Ab = 1.414\ m^2$

$e_y = \frac{I_s}{y_s * Ab}$

$e_y = \frac{0.0695}{\mathbf{2.75*10^2} * 1.414}$

$e_y = \mathbf{0.00185\ m}$

4.7.4 Hydraulic moment

$Fr = 3.58 * 10^6 \text{N}$

$e_y = 0.00185\ m$

$M_h = Fr * e_y$

$M_h = (\mathbf{3.58 * 10^6 N}) * (\mathbf{0.00185\ m})$

$M_h = \mathbf{6.53 * 10^3 Nm}$

5 Pressure

$Fw = 3.58 * 10^6 \text{N}$

$A = 1.414\ \text{m}^2$

$$P = \frac{F}{A} = \frac{F}{\frac{\pi\left(Dr^2 - Dh^2\right)}{4}} = \frac{3.58*10^6}{\frac{\pi\left(1.55^2 - 0.775^2\right)}{4}} = \mathbf{2.53 Mpa}$$

APPENDIX B

Matlab Code

```
clc
clear all

% Inputs
p = input('Power output (KW):\n'); % Power output in KW
Hop = input('operational Head Available (m):\n'); % operational Head
Available in m
H = input('Head Available (m):\n'); % Head Available in m
Hn = input('NetHead Available (m):\n'); % NetHead Available in m
H1 = input('Head one Available (m):\n'); % Head Available in m
H2 = input('Head two Available (m):\n'); % Head Available in m
At = input('Atmospheric Pressure (pa):\n'); % Atmospheric Pressure in pa
Vp = input('Vapor pressue of Water (pa):\n'); % Vapor pressue of Water in pa
C4 = input('Outlet Average velocity (m/s):\n'); % Outlet Average velocity in
m/s
eff = input('Overall Efficiency:\n'); % Overall Efficiency
Z = input('Number of Blades:\n'); % Number of Blades
v_dot = input('Flow Rate (m3/sec):\n'); % Flow Rate m3/sec
N = input ('Rotational Speed of turbine (m-1):\n'); % Rotational Speed of
turbine in m-1
Dr = input ('Runner Diameter (m):\n'); % Runner Diameter in m
attack = input('Optimum Angle of Attack (deg):\n'); % Optimum Angle of Attack

density = 1000;
bladesections = 5; % For design

% Discharge
Q = p * 1000 / (eff * density * 9.81 * H);
% Characteristic factor
```

```
M = (2 * N * (pi * v_dot)) / ((2 * 9.81 * H) ^ 0.75);% M = characteristic
factor
% Diameter number
d =(( Dr * sqrt(pi))/ 2 ) * ((2 * Hop * 9.81) /(v_dot ^ 2))^ 0.25 ;% d =
Diameter Number

% Specific speed
Ns = 885.5 / (H ^ 0.25);
% Turbine speed
N = Ns * (H * 1.25) / (p ^ 0.5);
phi = 0.0242 * (Ns ^ (2 / 3));

Dr = 84.5 * phi * (H ^ 0.5) / (N);

m = 0.5; % m = Dh / Dr
Dh = m * Dr; % Dh = Hub Diameter
n = 2.294 / (Hn ^ 0.486);

% Cavitation cofficient = Cc
Cc = (1.5241  * (n ^ 1.41)) + (C4 ^ 2) / (2 * 9.81 * Hn );
% Suction Head = Hs
Hs = ((At / (density * 9.81)) - (Vp / (density * 9.81))) + ((C4 ^ 2) / (2 *
9.81) - (Cc * Hn));

% Tangential velocity of blade
U = pi * Dr * N;
% Absolute velocity at inlet
Cu1 = (H1 * 9.81) / U;
% Absolute velocity at outlet
Cu2 = (H2 * 9.81) / U;
% Relative velocity at inlet
Wu1 = (Cu1 - U);
% Relative velocity at outlet
Wu2 = (Cu2 - U);
% Tangential velocity of fluid flow
Cu_inf = ((H - Hs) * 9.81) / U;

% Relative velocity in the tangential direction
Wu_inf = Cu_inf - U;

flowarea = pi * ((Dr ^ 2) - (Dh ^ 2)) / 4;
% Relative velocity at in meridian direction
Wm = v_dot / flowarea;
% Relative velocity one
W1 = sqrt(Wu1 ^ 2 + Wm ^ 2) ;
% Relative velocity two
W2 = sqrt(Wu2 ^ 2 + Wm ^ 2 ) ;

% Tangential velocity
Cu_12 = Q / flowarea;
% Whirl velocity
D_avg = (Dr + Dh) / 2;
v_avg = pi * D_avg * N / 60;
Wu_12 = p * 1000 / (density * Q * v_avg);
```

```
s = linspace(1.3, 0.75, bladesections);
i = 1;

for D = linspace(Dh, Dr, bladesections)
    U = (pi * D * N) / 60;
    beta_1 = atand(Cu_12 / (U - Wu_12));
    beta_2 = atand(Cu_12 / U);
    beta_inf =  - atand(Wu_inf / (Wm));
    beta_11 =  - atand(Wu1 / (W1));
    beta_22 =  - atand(Wu2 / (W2));


    % Blade Spacing;
    t = (pi * D) / Z;
    chord = s(i) * t;
    theta = 180 - beta_1 + attack;
    naca = xlsread('naca.xlsx');
    x = naca(:, 1);
    y = naca(:, 2);
    x = x * chord;
    y = y * chord;
    x = x - (chord / 2);
    R = [cosd(theta) sind(theta); -sind(theta) cosd(theta)];
    rot_matrix = R * [x'; y'];
    X_chord = rot_matrix(1, :)';
    Y_chord = rot_matrix(2, :)';
    Z_chord = zeros(35, 1);
    figure
    plot(X_chord, Y_chord);
    set(gcf, 'Position', [0, 0, 800, 800])
    section = [X_chord, Y_chord, Z_chord];
    i = i + 1;
end
```

Matlab Figure After Run the Code

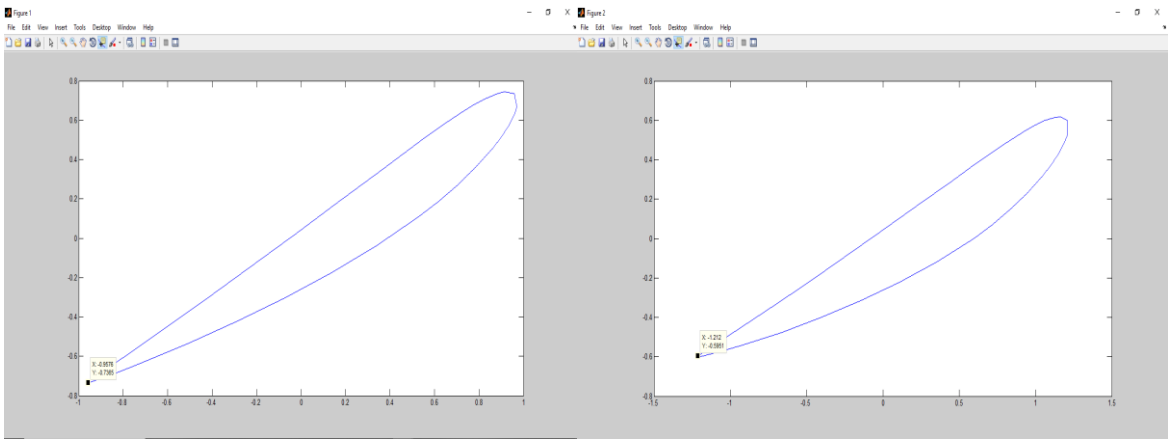

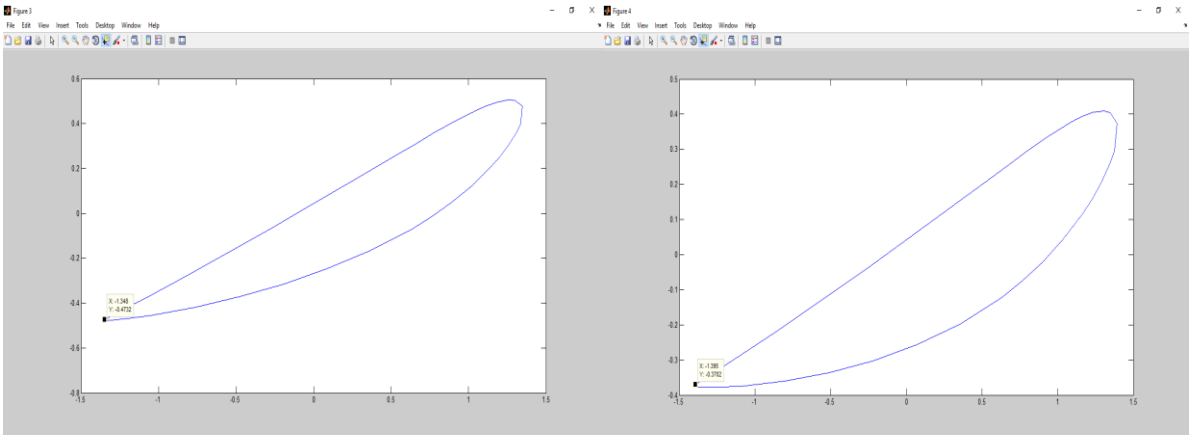

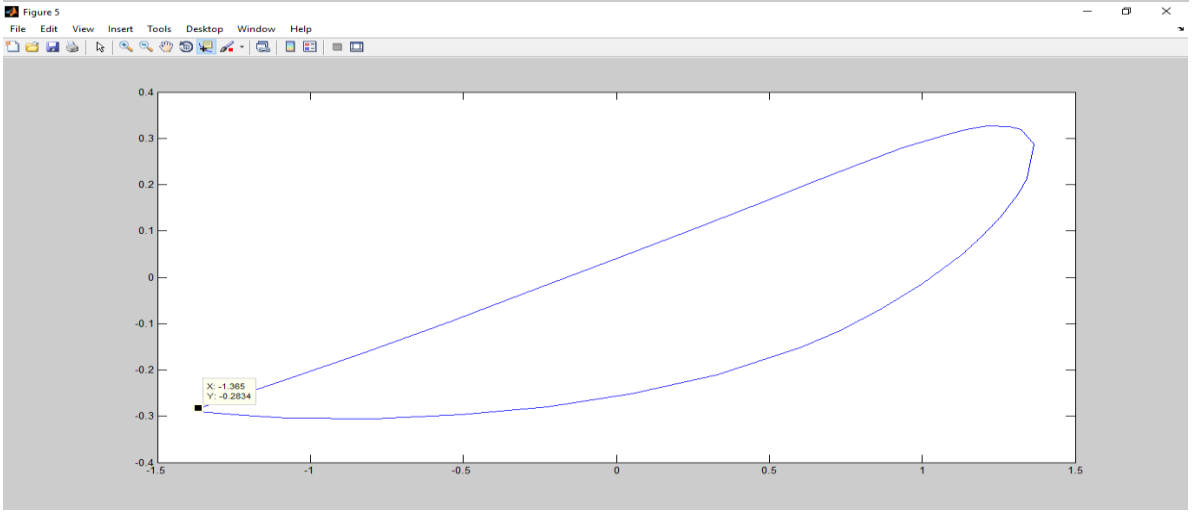

Text File for each airofoil shape

Figure 1 (Airofoil shape)

X	Y	Z
-0.9614	-0.7315	0
-0.8659	-0.6575	0
-0.7709	-0.583	0
-0.5814	-0.4329	0
-0.3934	-0.2811	0
-0.2066	-0.1276	0
-0.02055	0.02687	0
0.1655	0.1813	0

Figure 2 (Airofoil shape)

X	Y	Z
-1.212	-0.5951	0
-1.091	-0.5345	0
-0.9711	-0.4733	0
-0.731	-0.3495	0
-0.492	-0.2236	0
-0.2541	-0.09543	0
-0.01675	0.0339	0
0.2206	0.1632	0

Figure 3 (Airofoil shape)

X	Y	Z
-1.348	-0.4732	0
-1.214	-0.4247	0
-1.08	-0.3754	0
-0.8119	-0.2755	0
-0.545	-0.1732	0
-0.2789	-0.06841	0
-0.01335	0.03771	0
0.2522	0.1438	0

0.3506	0.337	0	0.4572	0.294	0	0.5172	0.2516	0
0.4431	0.415	0	0.5754	0.3596	0	0.6496	0.3057	0
0.5355	0.493	0	0.6936	0.4253	0	0.782	0.3598	0
0.6294	0.5691	0	0.813	0.4885	0	0.9154	0.4113	0
0.7256	0.6421	0	0.9343	0.5478	0	1.05	0.4584	0
0.7754	0.6765	0	0.9962	0.5748	0	1.119	0.479	0
0.827	0.7084	0	1.06	0.5987	0	1.188	0.4961	0
0.8829	0.7347	0	1.127	0.6155	0	1.261	0.5054	0
0.9145	0.7431	0	1.163	0.6179	0	1.3	0.5033	0
0.9595	0.734	0	1.211	0.5982	0	1.347	0.4767	0
0.9714	0.6688	0	1.21	0.5242	0	1.336	0.3991	0
0.9613	0.6322	0	1.91	0.4862	0	1.312	0.3616	0
0.933	0.5698	0	1.46	0.4239	0	1.257	0.3016	0
0.9002	0.5133	0	1.098	0.369	0	1.2	0.25	0
0.8644	0.4607	0	1.047	0.319	0	1.14	0.2039	0
0.7875	0.3624	0	0.9418	0.2277	0	1.018	0.1212	0
0.7049	0.2715	0	0.8317	0.1459	0	0.892	0.04898	0
0.6179	0.1864	0	0.7179	0.07128	0	0.7632	-0.01513	0
0.5271	0.1063	0	0.601	0.002983	0	0.6318	-0.07223	0
0.3358	-0.04127	0	0.3594	-0.1176	0	0.3628	-0.1686	0
0.1349	-0.1764	0	0.11	-0.2225	0	0.08762	-0.2476	0
-0.07241	-0.303	0	-0.1447	-0.3167	0	-0.1918	-0.3146	0
-0.2858	-0.422	0	-0.4042	-0.4013	0	-0.475	-0.3709	0
-0.5039	-0.5342	0	-0.6679	-0.4773	0	-0.7615	-0.4178	0
-0.7278	-0.6392	0	-0.9361	-0.5442	0	-1.052	-0.4544	0
-0.842	-0.6888	0	-1.072	-0.574	0	-1.198	-0.4686	0
-0.9576	-0.7365	0	-1.1259	-0.6701	0	-1.346	-0.4802	0

Figure 4 (Airofoil shape)

X	Y	Z
-1.395	-0.3702	0
-1.256	-0.332	0
-1.117	-0.293	0
-0.8393	-0.2134	0
-0.5625	-0.1314	0
-0.2863	-0.04689	0
-0.01047	0.03903	0
0.2653	0.125	0
0.5407	0.2126	0
0.6783	0.2566	0
0.8159	0.3007	0
0.9543	0.342	0
1.094	0.3788	0
1.164	0.3942	0
1.236	0.4059	0
1.31	0.4095	0
1.348	0.4044	0
1.394	0.3739	0
1.377	0.2965	0
1.35	0.2607	0
1.29	0.2046	0
1.228	0.1572	0
1.164	0.1154	0
1.035	0.04173	0
0.9022	-0.02103	0
0.7674	-0.07542	0

Figure 5 (Airofoil shape)

X	Y	Z
-1.365	-0.2834	0
-1.229	-0.2539	0
-1.093	-0.2235	0
-0.8207	-0.1615	0
-0.5494	-0.09704	0
-0.2786	-0.0301	0
-0.00803	0.03819	0
0.2625	0.1065	0
0.5327	0.1764	0
0.6677	0.2117	0
0.8027	0.2469	0
0.9383	0.2794	0
1.075	0.3076	0
1.144	0.3186	0
1.213	0.3262	0
1.285	0.3258	0
1.322	0.3188	0
1.364	0.2869	0
1.344	0.2132	0
1.315	0.1801	0
1.255	0.1292	0
1.193	0.08674	0
1.129	0.04975	0
1	-0.0144	0
0.8689	-0.06792	0
0.736	-0.1133	0

0.6306	-0.1226	0
0.3521	-0.1985	0
0.06872	-0.2562	0
-0.2179	-0.3017	0
-0.5076	-0.3361	0
-0.7998	-0.3607	0
-1.095	-0.3747	0
-1.244	-0.3775	0
-1.393	-0.37748	0

0.6016	-0.1515	0
0.3291	-0.21	0
0.05274	-0.2507	0
-0.2261	-0.2795	0
-0.5072	-0.2973	0
-0.7904	-0.3056	0
-1.076	-0.3035	0
-1.219	-0.2983	0
-1.363	-0.2905	0

Solidwork 3D Model Using the above Text file